Gondwana Research 21 (2012) 901–927

Contents lists available at ScienceDirect

Gondwana Research

journal homepage: www.elsevier.com/locate/gr

Zircon and muscovite ages, geochemistry, and Nd–Hf isotopes for the Aktyuz metamorphic terrane: Evidence for an Early Ordovician collisional belt in the northern Tianshan of Kyrgyzstan

A. Kröner [a,b,*], D.V. Alexeiev [c], E. Hegner [d], Y. Rojas-Agramonte [a], M. Corsini [e], Y. Chao [f], J. Wong [g], B.F. Windley [h], D. Liu [b], A.A. Tretyakov [c]

[a] Institut für Geowissenschaften, Universität Mainz, D-55099 Mainz, Germany
[b] Beijing SHRIMP Centre, Chinese Academy of Geological Sciences, 26 Baiwanzhuang Road, 100037 Beijing, China
[c] Geological Institute, Russian Academy of Sciences, Pyzhevsky per. 7, 119017 Moscow, Russia
[d] Institut für Geo- und Umweltwissenschaften, Universität München, Theresienstrasse 41, D-80333 München, Germany
[e] U.M.R. 6526 Geosciences Azur, Université de Nice-Sophia Antipolis, Nice, France
[f] Key Laboratory of Isotope Geochronology and Geochemistry, Guangzhou Institute of Geochemistry, Chinese Academy of Sciences, Guangzhou 510640, China
[g] Department of Earth Sciences, The University of Hong Kong, Pukfalam Road, Hong Kong, China
[h] Department of Geology, University of Leicester, Leicester LE1 7RH, UK

ARTICLE INFO

Article history:
Received 7 March 2011
Received in revised form 18 May 2011
Accepted 21 May 2011
Available online 30 May 2011

Keywords:
Collision
Crustal-melt granitoids
Kyrgyzstan
Nd and Hf isotopes
Northern Tianshan
Zircon geochronology
Muscovite Ar-dating
Tectonic model
Zircon age

ABSTRACT

The Aktyuz metamorphic terrane in the Kyrgyz northern Tianshan consists of granitoid gneisses and migmatites with subordinate paragneisses, greenschists, presumed meta-ophiolites, and garnet amphibolite dykes that contain HP eclogite relicts. The gneisses and migmatites were previously considered to be Archaean and Palaeoproterozoic in age on the basis of α-Pb and U–Pb multigrain zircon dating. Zircons from a post-tectonic granite were previously dated at 692 ± 15 Ma, constraining the time of main deformation and metamorphism in the Aktyuz terrane to the Precambrian.

The chemical characteristics of most granitoid samples are consistent with melting of chemically evolved crustal material, which is supported by Nd and Hf isotopic data. Zircon U–Pb SHRIMP ages were obtained for the main varieties of metamorphic rocks, for a gabbro of a low-grade ophiolite complex and for several post-kinematic igneous rocks. In addition, metamorphic muscovite was dated by the ^{40}Ar–^{39}Ar method, and whole-rock Sm–Nd isotopic systematics were obtained on several granitoid rocks. Our magmatic zircon crystallization ages for granitoid gneisses in the Aktyuz and Kemin Complexes range from 778 ± 6 to 844 ± 9 Ma which we interpret to reflect the time of magmatic emplacement of the gneiss protoliths. These rocks reflect an episode of Neoproterozoic granitoid magmatism, which is also documented in southern Kazakhstan, the Kyrgyz Middle Tianshan, the Chinese Central Tianshan and the Tarim Craton. Nd and Hf isotopic systematics show these rocks to be derived from Mesoproterozoic to Archaean sources. The calc-alkaline composition of these rocks seems compatible with a subduction setting, but is most likely inherited from the source, therefore the tectonic scenario for emplacement of the gneiss protolith remains unknown. Two ages of 562 ± 7 and 541 ± 3 Ma and negative $\varepsilon_{Nd(t)}$-values for granitoid gneisses document a later crustal melting episode. Muscovite $^{40}Ar/^{39}Ar$ ages of ca. 470 Ma for Aktyuz gneisses constrain the main fabric-forming metamorphism to the Early Palaeozoic. A migmatitic paragneiss, which was previously interpreted as Palaeoproterozoic, contains detrital zircons with an age spectrum from 503 to 1263 Ma; the youngest grain suggests a maximum Cambrian age of protolith deposition. An ophiolitic metagabbro of the Kemin Complex yielded an Early Cambrian age of 531 ± 4 Ma, which is close to the age of ophiolites in the adjacent Djalair–Naiman belt of Kazakhstan, suggesting a possible genetic link. Two samples of quartz diorite from the post-kinematic Dolpran pluton yielded Early Ordovician zircon ages of 471.9 ± 3.5 and 472.0 ± 3.1 Ma. The presence of a 783 ± 7 Ma xenocrystic zircon points at Precambrian crust at depth, which may explain an earlier, discordant apparent age obtained by multigrain zircon dating of this pluton. Undeformed rhyolite and basalt in the East Kyrgyz Range, previously classified as Neoproterozoic and Cambrian, yielded Late Ordovician ages of 451.9 ± 4.6 and 448.9 ± 5.6 Ma respectively.

Our data imply that the Aktyuz terrane is not a single segment of continuous Precambrian continental crust but represents a complex amalgamation of Neoproterozoic continental and Early Palaeozoic ophiolitic slivers, which

* Corresponding author. Tel.: +49 6131 3922163; fax: +49 61313924769.
E-mail address: kroener@uni-mainz.de (A. Kröner).

1342-937X/$ – see front matter
doi:10.1016/j.gr.2011.05.010

were stacked together in a subduction and collisional setting. Large fragments of continental crust were subducted to HP eclogite-facies conditions, which led to eclogite metamorphism in the mafic dykes. The main deformational event occurred during the latest Cambrian to earliest Ordovician between 503 and 472 Ma.

1. Introduction

Recent studies in the Central Asia Orogenic Belt (CAOB) have demonstrated that many medium- to high-grade metamorphic assemblages that were previously considered to be Archaean or Palaeoproterozoic in age are, in fact, much younger and document high-grade events associated with terrane accretion and subduction during the Palaeozoic (Shatsky et al., 1999; Salnikova et al., 2001; Kozakov et al., 2002; Gladkochub et al., 2008; Demoux et al., 2009; Hegner et al., 2010; Alexeiev et al., in press; Rojas-Agramonte et al., 2011). These data significantly change our understanding of regional tectonic settings, geometry of individual terranes, sutures, and structural boundaries and have important implications for the overall structure and evolution of the Central Asian accretionary collage in the Palaeozoic. The area of our interest in southern Kazakhstan and the North Tianshan of Kyrgyzstan contains several HP metamorphic assemblages that were recently dated at ~480–490 Ma (Tagiri et al., 1995; Orozbaev et al., 2007; Togonbaeva et al., 2009; Alexeiev et al., in press). This evidence suggests that high-grade metamorphic terranes that were previously regarded as parts of coherent Precambrian microcontinents may rather represent heterogeneous accretionary collages or collisional belts. This conclusion requires more detailed studies of these terranes to understand their origin, architecture and mutual correlation. We present single zircon ages, $^{40}Ar/^{39}Ar$ ages on muscovite, geochemical data, as well as Nd and Hf isotopic data of metamorphic and igneous rocks located in the Aktyuz area of the Kyrgyz northern Tianshan, considered to be part of the North Tianshan microcontinent (Bakirov and Maksumova, 2001; Windley et al., 2007). Our results provide new constraints for the reconstruction and understanding of this poorly known Early Palaeozoic collisional belt.

Previous zircon ages in the Kyrgyz northern Tianshan were either obtained by the α-Pb method (Larsen et al., 1952; Bowen, 1988) or by conventional multi-grain dating, often involving hundreds of grains per analysis. These mostly discordant analyses were also not based on previous cathodoluminescence imaging, and their significance and interpretations are therefore ambiguous (e.g., Kiselev et al. 1993).

2. Geological outline of the northern Tianshan in southern Kazakhstan and Kyrgyzstan

Kazakhstan and the Tianshan represent a complex amalgamation of Palaeozoic island arcs, accretionary complexes and Precambrian microcontinental terranes. These units were welded together during the Early Palaeozoic and were incorporated into Eurasia after collisions with Siberia, Baltica and Tarim in the Late Carboniferous and Permian (Zonenshain et al., 1990; Mossakovsky et al., 1993; Windley et al., 2007; Glorie et al., 2011) (Fig. 1). Archaean to Neoproterozoic metamorphic and igneous rocks are widespread in this wide, amalgamated domain (Filatova, 1993; Mossakovsky et al., 1993). Stratigraphic similarities and correlations of cover sequences outline two coherent microcontinents, namely the Ishim–Middle Tianshan microcontinent in the West and Southwest, and the Aktau–Junggar microcontinent in the East (Fig. 1). These are dominated by carbonate and fine-grained marine sediments with subordinate siliciclastic rocks which constitute continuous sections from the Neoproterozoic to Middle Ordovician (Nikitin, 1972; Degtyarev, 2003).

The Kokchetav–North Tianshan belt (KNT), situated between two large microcontinents (Fig. 1), represents an agglomeration of smaller blocks with Precambrian continental crust, high-grade metamorphic terranes, and Early Palaeozoic ophiolites. The Precambrian blocks in the Kokchetav–North Tianshan mainly consist of granitoid gneisses, some with Grenvillian ages of ~1.1 Ga (Kiselev, et al., 1993; Letnikov et al., 2007; Kröner, et al., 2009) and subordinate Palaeoproterozoic and Archaean rocks in southern Kazakhstan (Kröner et al., 2007). Cambrian to Early Ordovician ophiolites and associated sedimentary and volcanic rocks either form well delineated belts such as Dzhalair–Naiman (Fig. 1) or occur as chains of dismembered fragments between the Precambrian terranes (e.g., northern Kazakhstan and northern Tianshan) (Avdeev and Kovalev, 1989; Mikolaichuk et al., 1997; Degtyarev, 2003; Ghes' 2008; Qian et al., 2009; Alexeiev et al., in press). High-grade metamorphic rocks in the KNT were generally interpreted to be Precambrian in age although recent studies revealed Early Palaeozoic HP rocks in the Kokchetav region (Shatsky et al., 1999), in the Makbal area of the Kyrgyz northern Tianshan (Tagiri, et al., 1995; 2010; Togonbaeva et al., 2009) and the Anrakhai Mountains of southern Kazakhstan (Alexeiev et al., in press). The structure of the Kokchetav massif of the KNT is well documented as a flat-lying extrusion wedge cored by ultrahigh-pressure rocks that have peak metamorphic ages of 540–520 Ma (Katayama et al., 2001; Parkinson et al., 2002). An Early Ordovician unconformity in the Chu–Yili Mountains, the northern Tianshan, and in northern Kazakhstan (Abdulin 1980; Avdeev and Kovalev, 1989; Lomize et al., 1997; Mikolaichuk et al., 1997; Bakirov and Maksumova 2001; Korobkin and Smirnov, 2006; Ghes' 2008; Alexeiev et al., in press) implies that terranes with different origins and histories were amalgamated prior to the Late Arenigian (Dapingian).

3. Geology of the Aktyuz metamorphic terrane and previous geochronology

The Aktyuz metamorphic terrane is located in the southern KNT (Fig. 1) between the Latest Cambrian to Early Ordovician Dzhalair–Naiman ophiolite-bearing accretionary complex in the north (Bakirov and Maksumova, 2001; Ghes' 2008) and a Grenville-age granitoid gneiss terrane (Kochkorka Complex) in the south (Kiselev, et al., 1993; Kröner et al., 2009). It extends in an E–W direction for ~50 km in the Kyrgyz northern Tianshan (Fig. 2) and contains low-, medium- and high-grade metamorphic rocks which are exposed between Late Ordovician granitoids and middle to upper Palaeozoic igneous and sedimentary formations in the western part of the Zailiyskiy Ridge and the eastern part of the Kyrgyz Ridge (Fig. 2). Metamorphic rocks occur in two litho-tectonic assemblages, namely the Aktyuz and Kemin Complexes, which mainly differ from each other by the presence of HP rocks in the former. The Aktyuz Complex, exposed in the Kichi–Kemin River valley, east and west of Aktyuz village (Fig. 2), consists of well-foliated grey tonalitic to granodioritic gneisses (Fig. 3a) and pink granitic gneisses. Micaceous gneiss, schist, amphibolite, amphibole schist, quartzite and marble are minor (Bakirov, 1978; Bakirov et al., 2003). The entire assemblage is strongly deformed and displays a penetrative foliation in which intrafolial folds are rare, and all lithologies are structurally conformable. In high-strain zones granitoid gneisses have a thinly banded, regular, parallel fabric (Fig. 3b) produced by high-temperature ductile strain, and these rocks were previously mistakenly interpreted as metasediments. The folds in gneisses (Fig. 4d) trend east–west and indicate a top-to-the-south sense of motion (Bakirov, 1978).

Within the gneisses HP garnet amphibolites with rare cores of eclogite form conformable layers (ranging from 0.5 to 70 m in

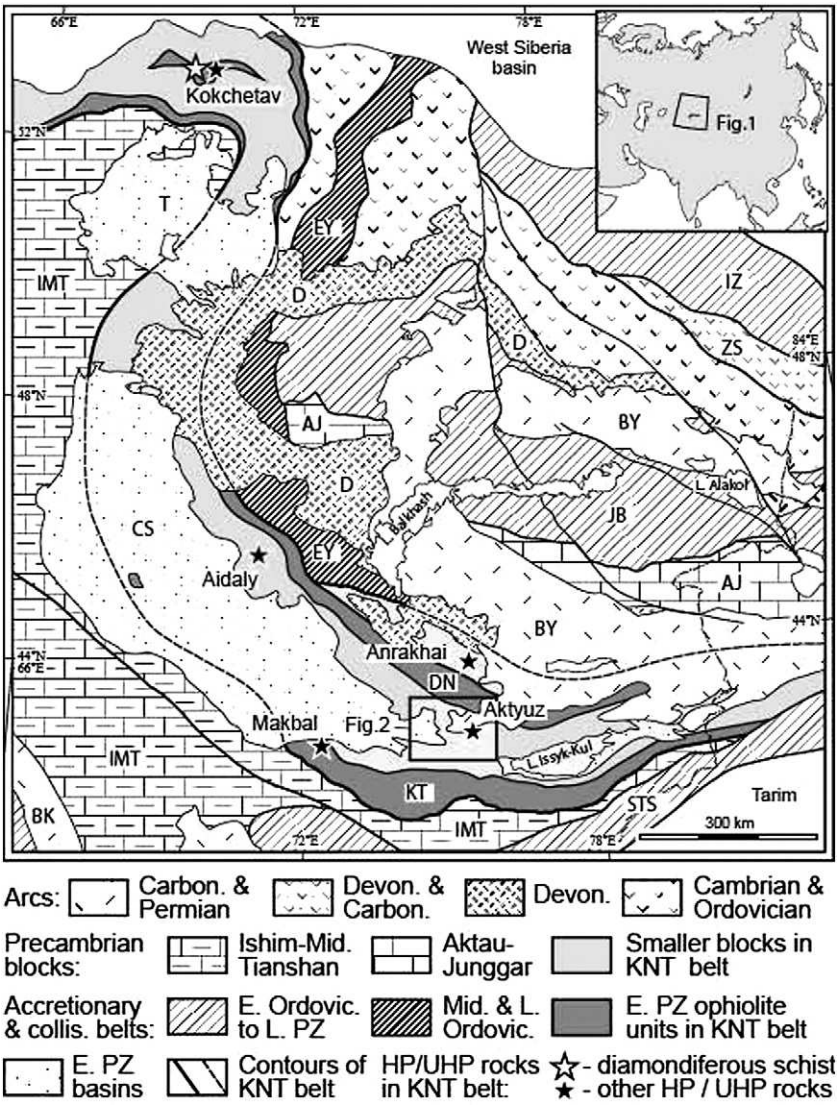

Fig. 1. Tectonic scheme of Palaeozoic Kazakhstan and the Tianshan (modified after Alexeiev et al., in press). Abbreviations for key domains–continental arcs: BY—Balkhash–Yili, BK—Beltau–Kurama; ZS—Zharma–Saur; D—Devonian Central Kazakhstan. Precambrian continental blocks: IMT—Ishim–Middle Tianshan; AJ—Aktau–Junggar. Accretionary and collisional belts: STS—South Tianshan; IZ—Irtysh–Zaisan; JB—Junggar–Balkhash, EY—Erementau–Yili, KNTS—Kokchetav–North Tianshan. Ophiolite belts: KT—Kyrgyz–Terskey, DN—Dzhalair–Naiman.

thickness and from 2 to 2000 m in length) sub-parallel to the foliation. In high-strain zones trains of boudinaged lenses suggest extreme extensional deformation of earlier layers (Orozbaev, et al., 2007, and references therein) (Fig. 4a). Orozbaev et al. (2010) determined a clockwise P–T path with peak metamorphic conditions at 550–660 °C and 21–23 kbar for the eclogites. Tagiri et al. (1995) and Orozbaev et al. (2007, 2010) suggested a Rb–Sr mineral/whole-rock isochron age of 749 ± 14 Ma to reflect retrograde metamorphism associated with uplift of the HP rocks. These authors also interpreted the amphibolites and eclogites as disrupted remnants of oceanic crust and considered their metamorphic evolution in terms of a hypothetical subduction-continent collision model. No evidence for oceanic crust was provided, and it is not clear which continents were invoked to have collided.

Results of our field work have shown that the amphibolite layers and boudins with relict eclogite mineralogy most likely represent a strongly metamorphosed and ductilely deformed gabbroic dyke swarm, because relict gabbroic igneous textures (Fig. 4b) and discordant contacts with the foliation of the host gneisses (Fig. 3a) are preserved in rare low-strain zones. The presence of gneiss xenoliths in the dykes (Fig. 4c) clearly shows that they were intruded into the surrounding granitoid gneisses. The HP rocks and the enclosing gneisses have been strongly retrogressed in the amphibolite-facies, and eclogitic remnants are only preserved in the centres of large boudins. The presence of discordant dyke contacts shows that the grey gneisses were already foliated prior to dyke injection and were then refoliated together with the dykes (Fig. 4d) during a high-grade event, which led to ductile fabrics with ubiquitous boudinage and almost complete parallelism of all lithologies. We compare the Aktyuz eclogitized dykes with similar occurrences elsewhere in the discussion below.

The Kemin Complex is exposed in the lower reaches of the Chon–Kemin and Kichi–Kemin Rivers and on the northern slope of the Kyrgyz Ridge, south of Orlovka village (Bakirov, 1978; see Fig. 2). It mainly consists of migmatitic paragneisses with subordinate amounts of granitoid gneisses and was subdivided into the Kapchigai and Kokbulak suites (Bakirov et al., 2003). The matrix of the migmatites in the Kapchigai suite consists of amphibolitic gabbro, ultramafic rocks, and cherty schists, which Bakirov et al. (2003) suggested to represent

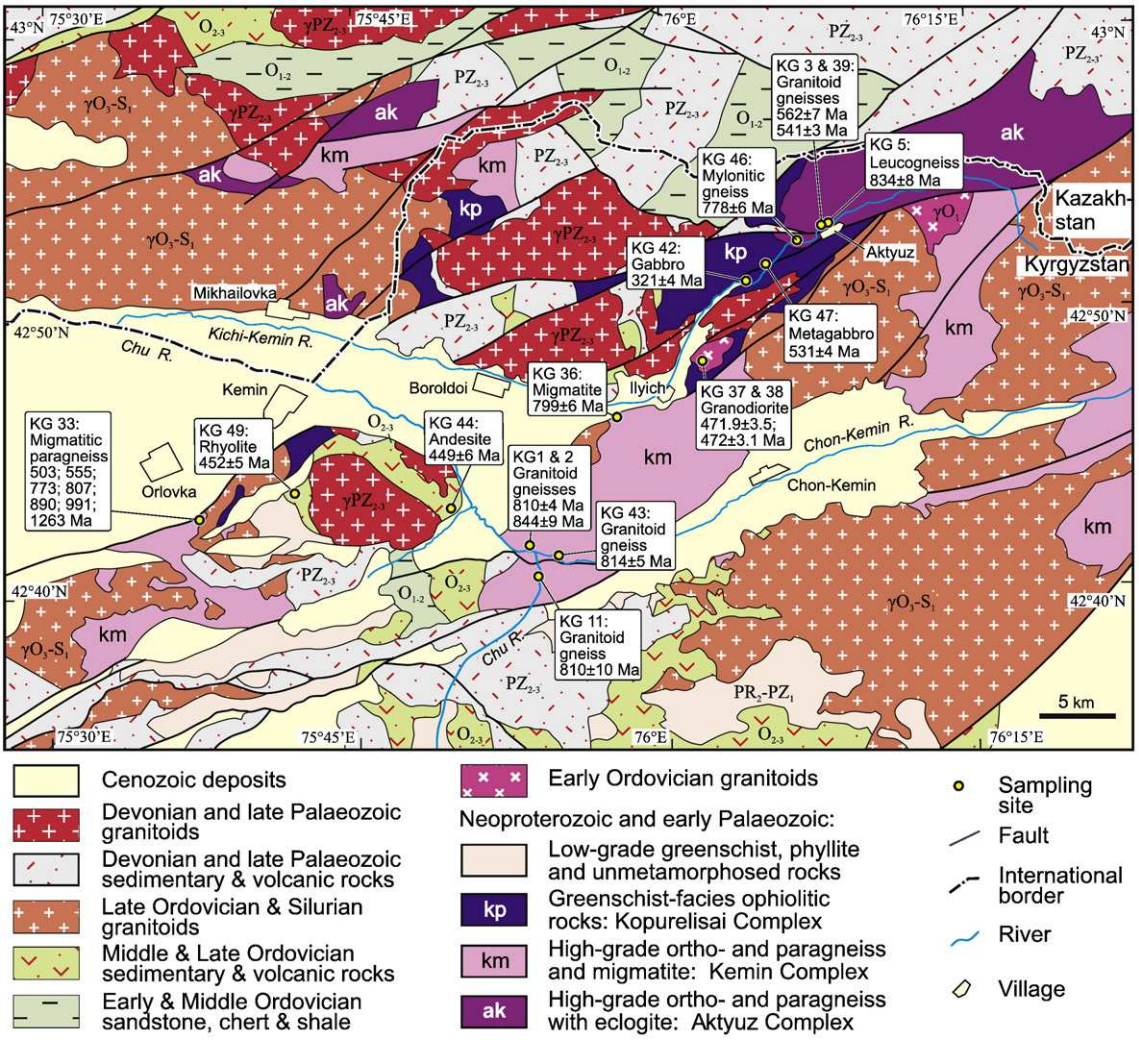

Fig. 2. Geological map of the Aktyuz and adjacent areas, compiled from Chakabaev (1979), Osmonbetov (1980) and unpublished maps of V.P. Morozov and I.V. Efremov. The sample localities and zircon ages of this study are indicated.

a metamorphosed ophiolite. The Kokbulak migmatites are interlayered with quartzite, graphite schist, marble, and paragneiss (Bakirov et al., 2003). Kokbulak migmatitic gneisses yielded α-Pb zircon ages of 2550 ± 250 and 2050 ± 200 Ma (Bakirov and Korolev, 1979), whereas migmatitic tonalitic–trondhjemitic gneisses in the lower reaches of the Chon–Kemin River suggested conventional multi-grain U–Pb zircon ages of ~2050 and 1850 ± 10 Ma with major scatter and discordancy of the data points (Kiselev et al., 1993).

In the middle segment of the Kichi–Kemin River presumed ophiolitic rocks of the Kopurelisai suite constitute a major block of the Kemin Complex (Bakirov et al., 2003; see Fig. 2). It is in thrust contact along a serpentinite mélange zone with tectonically overlying gneisses of the Aktyuz Complex (Bakirov et al., 2003; Ghes', 2008). The ophiolitic rocks include massive but foliated isotropic hornblende gabbro, greenschist-facies metabasalt, locally with well-preserved but flattened pillows. There are doleritic dykes and sills, but no sheeted dyke complex, plagiogranite, or layered gabbro have been found.

The interpretation of the Kopurelisai suite as a dismembered ophiolite is based on the observation of a combination of rock types commonly found in ophiolites such as serpentinite, gabbro, diabase, locally pillowed basalt, chert, and tuff. The rocks are strongly disrupted and metamorphosed, so primary relations are never preserved. There are no published age data for these greenschist-facies rocks, but Bakirov et al. (2003) suggested similarities with the much higher-grade and migmatized mafic rocks of the Kemin Complex of possible Palaeoproterozoic age, described above. Published chemical data of the metabasalts and actinolite schists show a large variation in composition, leading to ambiguous interpretations when it comes to origin and tectonic settings (Ghes', 2008).

The oldest stratified and unmetamorphosed sediments, exposed north of the Chon–Kemin and Chu River confluence, are Middle Ordovician (Llanvirnian) fossiliferous limestones (Bakirov and Mikolaichuk, 2009), which rest unconformably on the Kemin Complex and constrain the minimum age of metamorphism. In the Aktyuz area the oldest reported post-kinematic granitoid rocks (in the Kichi–Kemin valley) are granodiorites and quartz diorites of the Dolpran pluton (Fig. 2) for which conventional multi-grain U–Pb zircon dating yielded discordant data points with an upper Concordia intercept age of 692 ± 15 Ma (Kiselev et al. 1993). Based on the ages for metamorphic rocks and postkinematic granitoids, the main episode of deformation and metamorphism in the Aktyuz terrane was considered to be Precambrian, and the terrane was regarded as the metamorphic continental basement of the northern Tianshan or Muyunkum microcontinent (Bakirov, 1978; Bakirov et al., 2003).

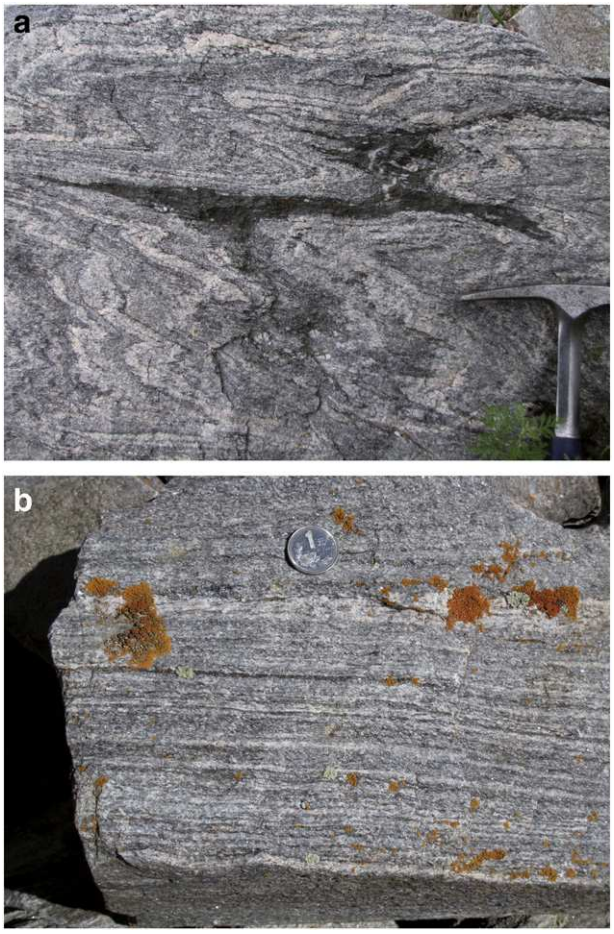

Fig. 3. Photographs of grey granitoid gneisses on S-facing Zailiyskiy Ridge in Kichi–Kemin River valley at Aktyuz. (a) Tightly folded banded gneiss including folded remnant of a mafic dyke in a low-strain zone. (b) Well-layered granitoid gneiss in high-strain zone.

4. Results

We undertook single zircon SHRIMP and muscovite $^{40}Ar/^{39}Ar$ dating, whole-rock chemical analyses, and a Sm–Nd whole-rock isotopic study of the major rock types in the Aktyuz Block in order to address the question of age, origin and position of metamorphic rocks in the Kyrgyz northern Tianshan. Precise ages were obtained for gneisses of the Aktyuz and Kemin Complexes, and an ophiolitic gabbro from the Kopurelisai suite. In addition, two samples of post-kinematic granite from the Dolpran pluton, a rhyolite and a basalt resting unconformably on the metamorphic rocks, and a post-tectonic gabbro intruding the Kopurelisai suite were dated in order to constrain the age of deformation and metamorphism. Data on sampling sites, rock types, geological association and age are summarized in Table 1, and the locations of dated samples are shown in Fig. 2.

The rock types dated in this study were analyzed for major and trace elements in the Guangzhou Institute of Geochemistry, Chinese Academy of Sciences, zircons were dated in the Beijing SHRIMP Centre, Chinese Academy of Geological Sciences, Sm–Nd isotopes were determined on whole-rock samples at Munich University, Germany, and single muscovite grains were dated by the $^{40}Ar/^{39}Ar$ method at Nice University, France, using the laser-probe step-heating technique. All analytical techniques are summarized in the Appendix.

4.1. Geochemical characteristics

The major and trace element concentrations of the samples discussed in this study are listed in Table 2 and are plotted in Figs. 5 and 6, and the data and chemical interpretations for the various geological units are summarized below.

4.1.1. Aktyuz and Kemin Complexes

The granitoid gneisses and migmatites of the Aktyuz and Kemin Complexes are mostly transitional metaluminous to peraluminous in composition (Fig. 5a). Migmatitic paragneiss sample KG 33 and mylonitic granite gneiss sample KG 46 with zircon-age evidence for inherited material (Table 1) have distinct peraluminous compositions and, by inference, comprise a significant sedimentary component. In the Ab–An–Or diagram of O'Connor (1965), the samples are of granitic to granodioritic composition and the peraluminous samples suggest a quartz monzonitic composition. All samples show high K_2O/Na_2O ratios (0.8 to 1.3 in the Kemin C., 1.2 to 3.1 in the Aktyuz C.), except for paragneiss sample KG 33, and enrichment of large-ion-lithophile elements. These chemical characteristics are consistent with melting of chemically evolved crustal material (Rudnik, 1995). This inference is well supported by an S-type affinity of the Aktyuz and Kemin samples as depicted in Fig. 5c.

Migmatitic paragneiss sample KG 33 plots outside the field for granitoid compositions, and apparently its composition has been modified by post-depositional (metamorphic?) processes. Several samples including KG 3, 33, 36, 39, 40, and 46 show a chemical affinity to A-type granitoids. For these samples the sum of high Zr, Nb, Ce, and Y concentrations versus the FeO^t/MgO and $(K_2O + Na_2O)/CaO$ ratios (Eby, 1992; Whalen et al., 1994 Whalen et al., 1987; Condie, 1991) consistently plots in the transitional region of I-type and A-type granites (not shown). Because a similar relationship can also be seen in the Pearce et al. (1984) diagrams and those using Ga/Al ratios (Whalen et al., 1987), we conclude that several of the Neoproterozoic gneisses have inherited A-type granitoid or within-plate components from their protoliths.

The REE patterns of the granitoids (Fig. 6a and b) show typical enrichment in the LREE and little fractionated HREE (except for granite-gneiss sample KG 2). The HREE patterns are consistent with melting of crustal sources lacking garnet, e.g. melting of mid- to upper crust at pressures less than 15 kbar during crustal thickening. Melting of deeper garnet-bearing sources is indicated for granite-gneiss KG 2 with moderately fractionated HREE. Some samples with large negative Eu-anomalies reflect the important role of plagioclase, probably during melt fractionation (Fig. 6a and b). Other samples with minute negative Eu-anomalies suggest protoliths (greywacke?) where plagioclase had been largely consumed during melting. In extended trace element variation diagrams (not shown) the samples show traits inherited from mature crustal sources such as negative anomalies for Nb, Ti, Sr, and P and a positive Pb anomaly.

Retrogressed eclogite sample KG 8 shows high FeO^t and TiO_2 concentrations of ca. 15.4 wt.% and 3.1 wt.%, respectively, combined with a low MgO content of ca. 5.7 wt.% ($FeO^t/MgO = 2.7$). These data suggest that the protolith was a chemically evolved tholeiitic ferrogabbro (Table 2). Ferrogabbros are typical rock types of a variety of tectonic settings such as propagating oceanic rifts, layered intrusions, and gabbroic complexes (Botcharnikov et al., 2008). A small positive Eu-anomaly (Fig. 6b) indicates some plagioclase accumulation in this sample so that its chemical composition cannot be interpreted simply as melt composition. A negative Nb-anomaly in KG 8 ($La/Nb = 1.4$) does not support a mid-ocean ridge or propagating oceanic rift setting and is compatible with a subduction environment and/or melt contamination in a continental setting. As tholeiitic ferrogabbros typically form under conditions of low oxygen fugacity, suppressing the crystallization of Fe–Ti phases, a fluid-rich subduction environment appears as an unlikely tectonic setting for the origin of

Fig. 4. Photos of field relationship of mafic dykes and enclosing granitic gneiss on Zailiyskiy Ridge at Aktyuz, northern Tianshan. (a) Boudin of gabbroic dyke in ca. 840 Ma granitoid gneiss. (b) Gabbroic texture in mafic dyke preserved in a low-strain zone. (c) Xenolith of granitic gneiss in a gabbroic dyke. (d) Granite-gneiss with lensoid fragment of mafic dyke, isoclinally folded together.

KG 8. We therefore suggest an intraplate environment where melt fractionation was accompanied by limited crustal melt contamination.

4.1.2. Kopurelisai ophiolite complex

Among the basaltic rocks of this complex, metagabbro sample KG 47 represents a cumulate with a large proportion of plagioclase as can be inferred from its high Al_2O_3 concentration of 19 wt.% and its positive Eu-anomaly (Fig. 6c). Basalt KG 48 with a SiO_2 concentration of 49 wt.% has a high FeO^*/MgO ratio of 1.6 suggesting a tholeiitic affinity (Miyashiro, 1974). The basalt sample has a flat REE pattern (Fig. 6c) with distinct subduction-related trace element signatures such as a negative Nb anomaly and positive anomalies for fluid-mobile elements such as Pb, Cs, Rb, Ba, and Sr (not shown). These characteristics are consistent with an origin in an immature oceanic island arc or a supra-subduction setting for the ophiolite. Similar chemical signatures were documented in earlier studies of the Kopurelisai Complex and of ophiolite sequences in the adjacent Dzhalair–Naiman and Kyrgyz Terskey ophiolitic belts of southern Kazakhstan and the northern Tianshan. In these cases the trace element data were interpreted as evidence for a possible back-arc origin (Lomize et al., 1997; Mikolaichuk et al., 1997; Ghes', 2008).

4.1.3. Post-kinematic felsic and mafic rocks

The little or undeformed post-tectonic Dolpran granodiorite samples KG 36 and 37 are metaluminous with a transitional granodioritic–tonalitic composition (Fig. 5a and b). These rocks show distinct calcic–alkalic I-type granite composition (Fig. 5c). They have low SiO_2 and high MgO concentrations (ca. 3.5 wt.%) and very low K_2O/Na_2O ratios of ca. 0.4 that attest to chemically depleted sources, such as the upper mantle and different from the middle-upper crustal sources for the Aktyuz and Kemin samples. The Dolpran samples show overall very low REE concentrations with negative anomalies for Nb and positive ones for Pb and the fluid-mobile elements Cs, Rb, and Ba (Fig. 6d). We suggest that these rocks were ultimately derived from melting of a subduction-modified upper mantle (final plate subduction or mantle lithosphere delamination during orogenic collapse?), followed by melt fractionation at crustal levels.

4.1.4. Burubai Formation

The chemical data for a Late Ordovician undeformed, flow-banded rhyolite (KG 49) and a basalt (KG 49a) are listed in Table 2. These samples were collected near the eastern termination of the Kyrgyz Range (Fig. 2, Table 1) and were previously correlated with the Neoproterozoic Bolshoi (Greater) Naryn Formation (Bakirov and Mikolaichuk, 2009). They are interpreted below as part of a volcanic arc sequence. Basalt sample KG 49a has a highly fractionated composition as can be inferred from its low MgO (4.6 wt.%) and Ni and Cr concentrations of <10 ppm. The basalt sample has a LREE-enriched pattern (Fig. 6e), augmented by subduction-related features such as a negative Nb, and positive anomalies for fluid-mobile elements Cs, Rb, Ba, and Pb (not shown). Melting of a subduction-

Table 1
Summary of sample localities, rock types, geological associations, and zircon ages for northern Tianshan samples, Kyrgyzstan.

Sample	N. latitude	E. longitude	Locality	Rock type	Complex/Formation	Age (Ma)
KG1	42°41′34″	75°52′55″	North bank of Chu River, west of confluence with Chon–Kemin River	Grey granitoid gneiss	Kemin Complex	844 ± 9
KG2	42°41′32.9	75°53′01.2″	North bank of Chu River, west of confluence with Chon–Kemin River	Red migmatitic granite-gneiss	Kemin Complex	810 ± 4.2
KG11	42°41′06.3″	75°53′23.3″	West bank of Chu River, south of confluence with Chon Kemin River	Foliated tonalitic gneiss	Kemin Complex	810 ± 10
KG33	42°42′49.2″	75°37′01.2″	Taldybulak River, south of Orlovka village	Migmatitic paragneiss	Kemin Complex	1263 ± 10 to 503 ± 8
KG36	42°46′17.1″	75°57′52″	Kichi–Kemin River, south of Dzhany–Dzhol village	Migmatite, some 80% granitic material	Kemin Complex	799 ± 6
KG43	42°41′23.5″	75°53′54.8″	North bank of Chon–Kemin River, east of confluence with Chu River	Grey granitoid gneiss	Kemin Complex	814 ± 5
KG3	42°52′55″	76°08′05″	Kichi–Kemin River, north of Aktyuz village	Granitoid gneiss	Aktyuz Complex	562 ± 7
KG5	42°52′55″	76°08′05″	Kichi–Kemin River, north of Aktyuz village	Well banded leucogneiss	Aktyuz Complex	834 ± 8
KG8	42°52′55″	76°08′05″	Kichi–Kemin River, north of Aktyuz village	Eclogite	Aktyuz Complex	Not dated
KG39	42°53′11.3″	76°07′37.8″	Kichi–Kemin River, north of Aktyuz village	Pink banded granitoid gneiss	Aktyuz Complex	540.8 ± 3.1
KG40	42°53′11.3″	76°07′37.8″	Kichi–Kemin River, north of Aktyuz village	Granite-gneiss with muscovite	Aktyuz Complex	not dated
KG46	42°52′20.4″	76°06′39.3″	Kichi–Kemin River, west of Aktyuz village	Mylonitic granite-gneiss	Aktyuz Complex	778 ± 6, 581 ± 4
KG42	42°50′59″	76°04′03″	Kichi–Kemin River, west of Aktyuz village	Unfoliated, coarse-grained leucogabbro		320.9 ± 4.1
KG47	42°51′44.7″	76°05′26.7″	Kichi–Kemin River, west of Aktyuz village	Foliated metagabbro	Kopurelisay Complex	531.2 ± 3.7
KG48	42°51′24.1″	76°04′59.2″	Kichi–Kemin River, west of Aktyuz village	Chloritized basalt	Kopurelisay Complex	Not dated
KG37	42°48′12.1″	76°01′32.8″	Kichi–Kemin River, east of Ilyich village	Foliated granodiorite/quartz-diorite	Dolpran Complex	471.9 ± 3.5
KG38	42°48′12.1″	76°01′32.8″	Kichi–Kemin River, east of Ilyich village	Unfoliated granodiorite/quartz-diorite	Dolpran Complex	472.0 ± 3.1
KG44	42°43′14.8″	75°49′54″	Some 400 m west of Cholok train station	Porphyritic basaltic andesite	Cholok Formation	448.9 ± 5.6
KG49	42°43′44.1″	75°41′28.9″	Eastern termination of Kyrgyz Ridge	Rhyolite	Burubai Formation	451.9 ± 4.6
KG49a	42°43′44.1″	75°41′28.9″	Eastern termination of Kyrgyz Ridge	Basalt	Burubai Formation	Not dated

modified mantle in an active arc or rift settings is indicated. The associated rhyolite sample shows similar subduction-related trace element characteristics as the basalt and may be related by crystal fractionation of a basaltic parental magma or, more likely, partial melting of a mafic crustal protolith similar to the basalt. The Late Ordovician and Early Silurian granites in the Kyrgyz northern Tianshan (Ghes', 2008; Konopelko et al., 2008; Glorie et al. 2010), show similar arc-related trace element characteristics as the rhyolite, and this similarity suggests that the volcanic rocks above may belong to the same magmatic belt.

4.2. Zircon U–Pb and muscovite $^{40}Ar/^{39}Ar$ ages, Sm–Nd whole-rock isotopic systematics, and zircon Lu–Hf isotopes

Precise dating of zircons less than about 1000 Ma in age by ion-microprobe and LA-ICP-MS is best achieved by using $^{206}Pb/^{238}U$-ages (see Black and Jagodzinski, 2003, for explanation) because the proportions of these two isotopes have changed by easily measurable amounts over most of that time, whereas the $^{207}Pb/^{206}Pb$ isotopic system is better suited to the dating of zircons older than about 1000 Ma because of the short half-life of ^{235}U producing ^{207}Pb (Black et al., 2003). We have followed this practice in quoting ages in this paper. Details of all analytical procedures for data in this paper are summarized in the Appendix. Sample locations are listed in Table 1 and Fig. 2, The SHRIMP analytical data are presented in Table 3, the Lu–Hf data in Table 4, the whole-rock Sm–Nd analyses in Table 5, and the $^{40}Ar/^{39}Ar$ step-heating results in Table 6.

4.2.1. Aktyuz Complex

Sample KG 5 is a strongly deformed, well foliated muscovite-rich, garnetiferous, grey, layered granitic gneiss collected on the south-facing slope of Zailiyskiy Ridge across the Kichi–Kemin River at Aktyuz village (Table 1). This is the main rock type along the ridge and it contains the mafic dykes described earlier. There is significant strain variation across the outcrop with low-strain zones exposing tight to isoclinally folded gneiss, occasionally including thin, streaky layers of amphibolite, which we interpret as intensely flattened mafic dykes (Fig. 3a). High-strain zones expose a regularly banded gneiss (Fig. 3b), dipping N at shallow angles, from which sample KG 5 was collected.

The dated sample consists of quartz, microcline, fresh albite, muscovite, epidote, a little chlorite and rare garnet. Muscovite and quartz aggregates are strongly aligned in the foliation, and there are a few large porphyroclasts of quartz and feldspar. The zircons are uniformly long-prismatic with slight rounding at their terminations, and the zircon morphology together with the well-developed oscillatory zoning as seen in CL images (Fig. 7a), clearly identifies the igneous origin of this rock. Eight grains were analyzed on SHRIMP II and produced well-grouped concordant results (Table 3) with a mean $^{206Pb}/^{238}U$ age of 834 ± 8 Ma (Fig. 7a), which we interpret to reflect the time of emplacement of the gneiss protolith.

Twenty-nine spots on well preserved zircons with clear oscillatory zoning were analyzed for their Lu–Hf isotopic compositions, including the eight grains analyzed on SHRIMP II, and the results are presented in Table 4, including depleted mantle extraction (t_{HfDM}) and crustal model ages (t_{Hfc}). Since the whole-rock $^{176}Lu/^{177}Hf$ ratio of the sample was not measured, an average crustal value of 0.010 was assumed (see explanation in the Appendix). This, together with considerable scatter in $\varepsilon_{Hf(t)}$-values for the measured magmatic age of 834 Ma, produces an array of t_{Hfc} ages which range from 1.71 to 2.38 Ga (Table 4, Fig. 8a). The most plausible explanation for this variation in isotopic composition and model age is that the gneiss protolith was derived from a very heterogeneous Palaeoproterozoic crustal source. Such heterogeneity has also been observed in other crustal-melt granitoids (e.g., Belousova et al., 2006; Phillips et al., 2011; Villaros et al., 2011; Kröner et al., 2012-this issue) and will be further discussed below.

A whole-rock sample of the gneiss was analyzed for its Sm–Nd isotopic systematics, and the $\varepsilon_{Nd(t)}$-value is −4.7 with a corresponding mean crustal residence age of 1.57 Ga (Table 5). This is consistent with the peraluminous, S-type character of the rock (Fig. 5) and can either be interpreted as reflecting generation from older crust formed during a depleted mantle melting event at about 1.53 Ga or mixing of

Table 2
Major and trace element concentrations for igneous rocks from the northern Tianshan orogenic belt of Kyrgyzstan.*

Sample no.	KG-1†	KG-2†	KG-11†	KG33‡	KG36‡	KG43‡	KG-3†	KG-5†	KG-8‡	KG-39‡	KG-40‡	KG-46‡	KG42‡	KG47‡
Complex	Kemin	Kemin	Kemin	Kemin	Kemin	Kemin	Aktyuz	Aktyuz	Aktyuz	Aktyuz	Aktyuz	Aktyuz	–	Kopu-relisay
Rock type	Granite-gneiss	Granite-gneiss	Tonalitic gneiss	Migmatitic paragneiss	Migmatite	Granitoid-gneiss (melanos.)	Granitoid gneiss	Banded leucogneiss	Eclogite	Pink granite-gneiss	Granite-gneiss with muscovite	Mylonitic granite-gneiss	Carbonif. gabbro	Meta-gabbro
SiO_2	66.86	73.11	66.60	59.61	70.79	64.83	76.27	75.21	45.09	75.57	67.00	75.18	49.64	48.37
TiO_2	0.55	0.24	0.50	1.03	0.31	0.57	0.14	0.29	3.07	0.24	0.63	0.21	1.45	0.71
Al_2O_3	14.83	13.41	15.24	17.53	13.03	15.56	11.79	12.52	15.18	12.54	15.16	13.07	17.95	19.40
Fe_2O_3	4.38	1.80	4.15	8.04	3.30	4.67	1.24	1.47	17.14	2.07	3.09	2.49	10.95	7.24
MnO	0.12	0.05	0.11	0.07	0.07	0.13	0.02	0.05	0.21	0.05	0.19	0.05	0.21	0.11
MgO	2.00	0.68	1.44	3.62	1.08	1.94	0.21	0.50	5.68	0.17	0.94	0.28	4.25	6.87
CaO	2.81	1.20	3.25	1.55	1.77	3.18	0.80	1.14	10.09	0.42	2.80	0.14	8.45	12.13
Na_2O	3.48	3.52	4.16	1.49	4.22	3.55	3.31	2.89	3.19	3.71	1.53	2.02	3.07	2.41
K_2O	3.27	4.47	3.42	4.61	3.26	3.08	4.89	4.73	0.30	4.58	4.69	4.54	1.62	0.36
P_2O_5	0.15	0.08	0.19	0.14	0.05	0.16	0.02	0.06	0.17	0.02	0.12	0.03	0.31	0.10
LOI	1.38	1.32	0.80	3.01	2.33	1.48	1.19	1.04	0.21	0.86	3.89	1.47	2.63	2.08
Total	99.83	99.88	99.86	100.70	100.21	99.15	99.88	99.30	100.33	100.23	100.04	99.48	100.33	100.80
Cs	1	0.3	0.5	6.6	0.3	0.6	0.8	1.1	n.d.	0.5	3.0	1.0	n.d.	0.3
Rb	95	74	63	163	53	69	110	103	n.d.	72	104	59	42	7.5
Sr	459	237	543	161	196	416	37	115	557	37	254	16	536	279
Ba	1387	876	1270	892	620	1250	557	1325	171	581	1563	619	693	116
Hf	4.58	3.69	4.75	5.26	6.56	3.97	7.46	4.86	2.71	6.24	7.16	3.55	b.d.	0.88
Zr	203	152	203	210	220	173	244	195	106	231	320	129	79	33
Ta	1.39	1.24	1.32	2.34	0.98	1.07	2.55	2.24	0.70	1.83	1.31	0.87	b.d.	0.17
Nb	15	7.6	11	24	14	13	24	15	4.2	19	16	9.3	7.0	1.4
Y	23	10	19	36	36	22	61	21	18	47	34	24	23	11
U	0.6	1.1	1.1	3.5	0.7	0.5	2.2	2.3	0.1	1.6	1.3	1.0	0.5	0.02
Th	8.3	16	7.2	24	8.7	7.9	16	14	0.4	11	8.1	5.5	1.1	0.1
Pb	11	1.9	0.3	6.5	5.9	3.5	3.5	4.0	11	1.0	4.5	2.5	5.0	4.9
Ga	15	12	15	21	15	13	18	13	n.d.	13	16	8.4	19	12
Cr	26	15	18	112	27	18	12	9.4	n.d.	6.9	8.4	6.9	14	392
Ni	11	7.8	10	51	15	9.4	4.8	4.5	n.d.	6.6	9.5	3.7	8.0	53
La	44.02	42.85	39.52	65.11	48.41	42.95	56.19	43.05	6.09	50.31	72.97	21.86	18	2.82
Ce	84.70	89.67	80.79	118.71	102.61	76.67	130.44	85.54	16.70	129.40	132.19	50.85	34	6.50
Pr	8.68	8.13	8.03	13.61	10.50	8.38	13.31	8.01	2.55	11.72	14.37	5.31	3	1.07
Nd	32.47	27.76	29.60	54.23	38.87	31.82	49.70	27.43	12.70	41.19	56.39	20.55	18	6.07
Sm	5.56	4.55	5.02	10.40	7.32	5.52	10.31	4.63	3.51	7.79	9.52	4.30	5	1.93
Eu	1.44	0.85	1.33	1.77	0.66	1.34	0.78	0.72	1.39	0.79	2.72	0.69	b.d.	0.83
Gd	5.11	3.30	4.25	8.63	5.86	4.51	9.73	3.92	3.86	7.03	7.73	4.01	2.00	2.17
Dy	4.40	2.15	3.73	6.96	6.77	4.00	10.87	3.66	3.92	8.01	6.40	4.29	n.d.	2.23
Ho	0.85	0.40	0.72	1.36	1.39	0.80	2.23	0.74	0.75	1.75	1.27	0.90	n.d.	0.44
Er	2.46	0.99	2.04	4.47	4.25	2.35	6.74	2.23	2.12	5.52	3.64	2.70	n.d.	1.22
Yb	2.65	0.88	2.09	4.26	4.31	2.40	6.64	2.50	1.87	5.95	3.69	2.79	n.d.	1.06
Lu	0.41	0.13	0.33	0.63	0.66	0.39	0.94	0.38	0.29	0.94	0.57	0.43	n.d.	0.16

SiO_2	49.34	58.78	55.29	47.45	74.34	47.56	58.57	50.20	58.84	49.90	–	54.4
TiO_2	1.21	0.53	0.66	1.05	0.11	1.01	1.06	0.29	1.05	0.29	–	2.27
Al_2O_3	13.74	17.78	18.54	18.21	13.31	18.69	16.96	20.61	17.15	20.69	–	13.4
Fe_2O_3	12.61	5.39	7.08	11.36	1.48	11.66	6.92	6.64	6.77	6.21	–	13.9
MnO	0.24	0.12	0.13	0.20	0.05	0.24	0.10	0.11	0.09	0.11	–	0.19
MgO	6.99	3.50	3.30	5.83	0.19	4.63	1.56	0.55	1.53	0.54	–	3.56
CaO	11.58	6.08	6.52	9.82	0.67	7.82	5.13	8.12	4.94	8.05	–	7.06
Na_2O	2.78	3.76	3.92	2.36	3.74	2.96	4.14	7.15	4.26	7.10	–	3.23
K_2O	0.15	1.48	1.63	1.48	4.28	1.74	2.89	1.66	2.92	1.66	–	1.74
P_2O_5	0.08	0.13	0.14	0.08	0.03	0.22	0.47	0.12	0.49	0.13	–	0.37
LOI	2.59	2.02	2.24	2.48	1.18	2.60	1.20	4.53	1.20	4.56	–	–
Total	100.14	99.23	99.45	100.32	99.38	99.13	99.85	100.03	99.24	99.24	–	–
Cs	0.2	1.2	1.2	n.d.	1.4	2.2	1.77	1.26	1.50	1.28	0.93	1.16
Rb	2.1	44	46	72	96	65	55	69	55.00	67.30	37.95	47
Sr	218	574	505	426	89	472	1176	643	1191.0	662.00	330	342
Ba	28	918	769	546	954	590	348	1232	340.00	1226.0	635	683
Hf	1.9	1.7	1.0	b.d.	3.61	2.0	11.09	5.04	10.60	5.10	5.45	4.84
Zr	65	56	30	92	119	70	506	222	517.00	227.00	206	184
Ta	0.2	0.8	0.7	n.d.	1.5	0.3	0.93	0.85	0.90	0.90	0.90	0.78
Nb	1.5	7.7	4.7	5	9.2	2.9	14.42	14.30	13.00	15.00	12.51	12.5
Y	28	11	17	23	17	23	118	19.28	119.00	20.00	37.60	35
U	0.04	1.6	0.7	3.3	2.4	0.8	0.85	1.86	0.80	1.92	1.39	1.69
Th	0.2	2.4	1.7	4.0	16	3.9	1.47	6.27	1.40	6.50	6.74	5.9
Pb	6.8	8.1	14	26	4.4	8.2	10.89	35.11	–	36.00	9.16	11
Ga	12	15	14	20	9.6	14	35	20.69	35.00	20.00	17.53	23
Cr	77	87	1	32	8.8	3.8	12.59	10.50	12.00	10.10	12.48	17
Ni	41	27	5.23	15	5.3	11	8.06	15.07	–	16.00	1.,50	13
La	3.01	9.99	11.36	11	29.60	12.67	59.05	39.14	58.00	38.00	26.07	24.7
Ce	8.34	19.15	22.33	23.0	51.56	24.52	124.52	69.85	122.00	67.00	46.27	53.3
Pr	1.51	2.34	2.70	0	5.19	3.42	15.21	8.90	15.00	7.60	6.40	6.7
Nd	8.81	10.20	12.18	12	18.21	16.02	60.90	33.66	57.00	33.00	29.84	28.9
Sm	3.14	2.31	2.73	4	3.26	4.38	12.76	5.79	12.70	5.90	7.04	6.59
Eu	1.17	0.76	0.87	n.d.	0.48	1.35	2.04	1.49	2.00	1.64	1.98	1.97
Gd	4.07	2.08	2.73	2.00	2.68	4.35	14.48	4.83	14.00	5.00	7.24	6.71
Dy	5.08	2.10	3.14	n.d.	2.85	4.42	18.75	3.69	18.20	3.60	7.23	6.44
Ho	1.10	0.43	0.64	n.d.	0.59	0.87	4.35	0.65	4.30	0.67	1.47	1.27
Er	3.14	1.32	1.86	n.d.	1.82	2.54	14.49	1.84	14.20	1.70	4.16	3.7
Yb	2.92	1.38	2.02	n.d.	2.06	2.37	14.47	1.63	14.80	1.72	3.86	3.39
Lu	0.43	0.21	0.30	n.d.	0.33	0.38	2.34	0.25	2.10	0.27	0.58	0.503

b.d. = below detection limit, n.d. = not determined, rec. = recommended value.

* Major elements are in wt.%, trace are elements in ppm.

† Analyses were performed in Mainz.

‡ Analyses were performed in Guangzhou.

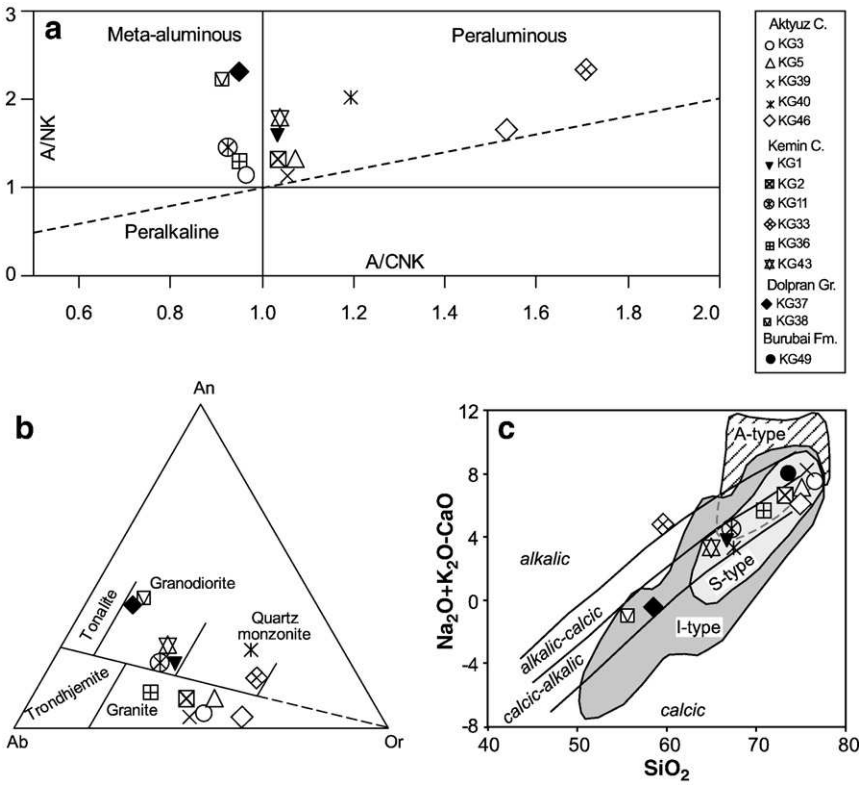

Fig. 5. Chemical characterization of granitoid rocks from the Aktyuz–Kemin and post-tectonic Dolpran complexes, northern Tianshan of Kyrgyzstan. (a) Shand (1943) plot; A/CNK = molecular ratio $Al_2O_3/(CaO + Na_2O + K_2O)$; A/NK = molecular ratio $Al_2O_3/(Na_2O + K_2O)$ (b) Normative feldspar compositions after of O'Connor (1965); (c) Granitoid classification of Frost et al. (2001).

unspecified older crust with a juvenile input. The presence of muscovite and garnet in the gneiss implies that a sedimentary source was involved in the generation of its protolith. Note, however, that the Nd mean crustal residence age is younger than the range of zircon t_{Hfc} model ages shown in Table 4 and Fig. 8a, and this may either mean that a young component is present in the gneiss which is not reflected in the zircons, or the Sm–Nd system was decoupled from the Lu–Hf system, possibly through metamorphic disturbance, as has been observed elsewhere (e.g., Hoffmann et al., in press).

The above grey muscovite-rich gneiss is interlayered with a less voluminous pink, medium- to coarse-grained K-feldspar-rich granite-gneiss in which we did not find mafic dykes, and despite intensive search no intrusive relationships could be established in the field. We have sampled two varieties of this gneiss: KG 3 is coarse-grained and was taken a few metres away from KG 5, KG 39 is medium-grained with more pronounced layering and was taken higher up the slope of the Zailiyskiy Ridge, some 400 m farther to the NW (Table 1, Fig. 2). KG 3 is well foliated and consists of quartz, microcline, marginally seriticized albite, biotite and a little muscovite. Some large porphyroclasts of quartz and microcline occur in the fine-grained partly mylonitized groundmass. Sample KG 39 has a similar composition. The zircons in both samples are virtually identical, and long-prismatic varieties with slight rounding at their terminations predominate. CL images reveal well-developed oscillatory zoning of magmatic origin (Fig. 7b and c, insets), and no older cores were seen in these grains. Six grains were analyzed in each sample, and the concordant results are well grouped in both cases (Table 3), yielding mean $^{206}Pb/^{238}U$ ages of 562 ± 7 (Fig. 7b) and 540.8 ± 3.1 Ma (Fig. 7c). In view of the igneous nature of the zircons we interpret these ages to reflect emplacement of the gneiss protoliths. Although the age difference is not large, the samples appear to reflect distinct granitic phases. Both the grey and pink gneisses share the same foliation, which was produced during a high-strain ductile deformation event, presumably under high-grade metamorphic conditions in the lower crust, and this event must be younger than ca. 541 Ma.

The $\varepsilon_{Nd(t)}$ value for whole-rock sample KG 3 is −4.8, and the corresponding mean crustal residence age is 1.53 Ga (Table 5), similar to sample KG 5. The same interpretation as for KG 5 can be advanced, i.e. the gneiss protolith is a crustal-melt granite, and it is most likely that both gneiss precursors were derived from broadly the same crustal source.

Retrogression of the Aktyuz mafic dykes was facilitated by extensive mylonitization that also affected the granite-gneisses, which developed broad zones of muscovite- and biotite-rich gneiss, locally grading into fissile schist. These rocks were mistakenly interpreted as clastic metasediments by previous authors. We collected sample KG 46 from such a zone (Fig. 9) in the valley of the Kichi–Kemin River, some 2 km W of Aktyuz (Table 1, Fig. 2). The sample has a granitic composition (Table 2) and is rich in well-oriented muscovite, and the mylonitic fabric is also evident through the strong alignment of fragmented quartz and feldspar aggregates.

The zircons are mostly short-prismatic with some rounding at their terminations and they display oscillatory zoning (Fig. 7d). Overall, these grains are similar to those in the above granite-gneisses. Five zircons were analyzed (Table 3), and four analyses are concordant and well grouped, providing a mean $^{206}Pb/^{238}U$ age of 778 ± 6 Ma (Fig. 7d), which we relate to the time of protolith emplacement. Although this sample is distinctly younger than KG 5 we consider it to reflect the same event of granitoid magmatism, and we shall show in the Discussion below that this event is also widespread in the Chinese Tianshan and seems to cover a time range from about 750 to 850 Ma. One euhedral grain, optically indistinguishable from the others and with oscillatory

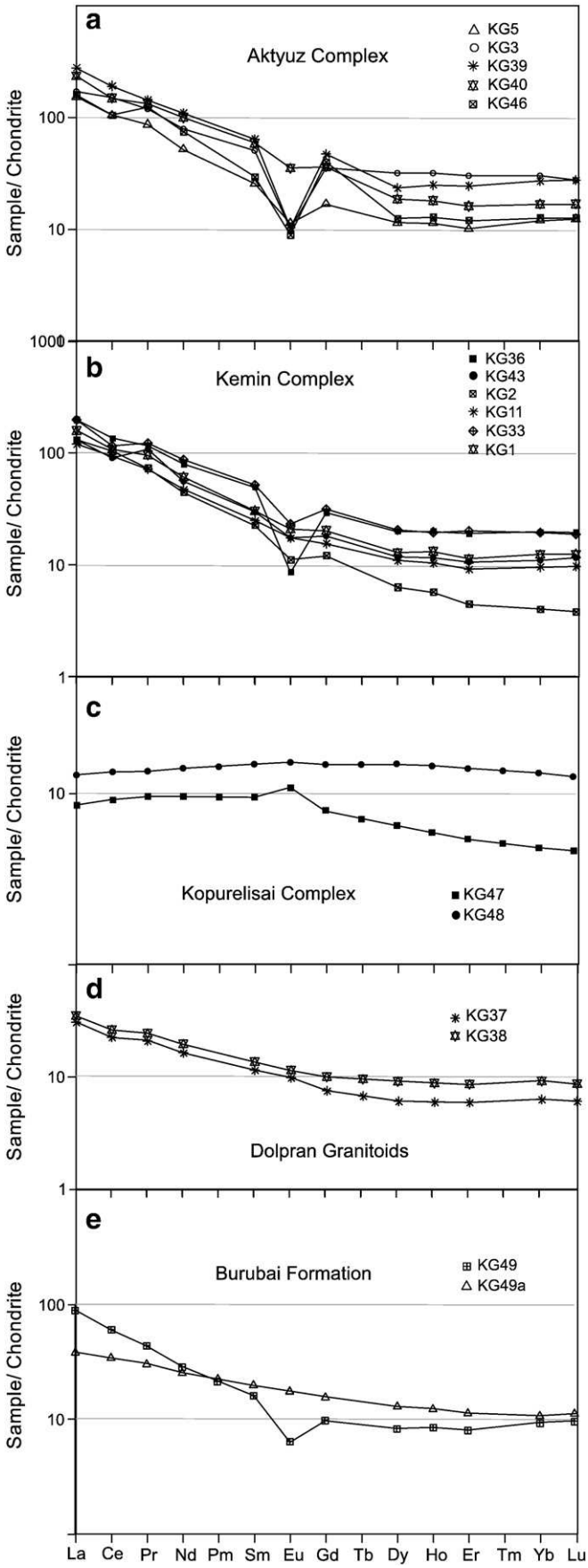

Fig. 6. Chondrite-normalized REE patterns for granitoid and mafic rocks of the Aktyuz (a), Kemin (b), Kopurelisai (c), Dolpran (d), and Burubai (e) geological units. Normalizing values from Nakamura (1974).

zoning, provided a much younger, concordant age of 581 ± 4 Ma (Table 3, Fig. 7d). We tentatively consider this grain to reflect a phase of younger granitic magmatism as recorded in samples KG 3 and KG 39, but the precise relationships cannot be reconstructed in this high-strain, retrograded rock. The important message from this sample is that it contains no detrital zircons and thus confirms our field interpretation that it is a sheared and retrograded granite-gneiss.

Two muscovite-rich samples from the Aktyuz granitoid assemblage were selected for $^{40}Ar/^{39}Ar$ dating in order to define the age of the main fabric-forming event in these rocks. Sample KG 40 is from the same locality as KG 5 and contains abundant, thin muscovite flakes which are oriented parallel to the main foliation/compositional banding defined by elongate crystals and "augen" of K-feldspar and quartz. Sample KG 46 is the strongly downgraded and mylonitized, fissile rock shown in Fig. 10 and from which zircons were dated.

The Ar-data are listed in Table 6 and are shown in the degassing spectra of Fig. 10 and exhibit well defined plateaux with ages of 470.6 ± 5.3 and 475.7 ± 5.5 Ma respectively. These are interpreted to reflect the time of closure of the Ar isotopic system in the muscovite grains during retrograde metamorphism. By implication, this age is also close to the time of the main fabric-forming event in the Aktyuz gneisses.

4.2.2. Kemin Complex

Sample KG 1 is a grey, medium-grained, finely-layered, isoclinally folded, granodioritic gneiss collected in the Chu River valley from a road cut on the road to Chon–Kemin (Table 1, Fig. 2). It consists of undulous quartz, microcline, little albite, much biotite and epidote. No muscovite was observed in this sample. The zircons are mostly euhedral with slight rounding at their terminations, and Cl images show well developed oscillatory zoning. Many grains exhibit very thin low-luminescence (low-U) rims that probably represent metamorphic overgrowths (Fig. 11a, inset) but they are too narrow for SHRIMP analysis. The magmatic cores of seven grains were analyzed and yielded concordant, well-grouped results (Table 3) that define a mean $^{206}Pb/^{238}U$ age of 844 ± 9 Ma (Fig. 11a). In view of the magmatic nature of the zircons we interpret this age as reflecting the time of granodiorite emplacement. The compatibility of this result with the 834 ± 8 Ma age of Aktyuz Complex sample KG 5 confirms the long-established correlation of the Aktyuz and Kemin Complexes.

Ten spots on zircons with clear oscillatory zoning were analyzed for their Lu–Hf isotopic compositions, including the seven grains analyzed on SHRIMP II, and the results are presented in Table 4. As in sample KG 5, there is scatter in the $\varepsilon_{Hf(t)}$-values for the measured magmatic age of 844 Ma which produces an array of t_{Hfc} ages ranging from 2.40 to 2.60 Ga (Table 4, Fig. 8b). However, this scatter is considerably smaller than in KG 5 and suggests a less heterogeneous, Early Palaeoproterozoic to Neoarchean crustal source for the gneiss protolith.

The $\varepsilon_{Nd(t)}$ value for whole-rock sample KG 1 is −11.2 and the corresponding mean crustal residence age is 2.04 Ga (Table 5), the second oldest of our samples analyzed in this study. The Nd isotopic data also confirm that the gneiss protolith was a crustal-melt granodiorite, consistent with its peraluminous, S-type character (Fig. 5) and, as in the case of the Aktyz gneiss, the Nd data can either be interpreted as reflecting generation from Palaeoproterozoic crust formed during a depleted mantle melting event or mixing of unspecified older crust with juvenile magma. Note, however, that the Nd mean crustal residence age is again significantly lower than the zircon t_{Hfc} model ages, and the same explanation as advanced for KG 5 may apply.

Table 3
SHRIMP zircon analyses from rocks of the Aktyuz and Kemin Complexes, northern Tianshan, Kyrgyzstan. For analytical details see Appendix. Errors in isotopic ratios are 1-sigma absolute.

Sample #*	U ppm	Th ppm	$^{206}Pb/^{204}Pb$	$^{208}Pb/^{206}Pb$	$^{207}Pb/^{206}Pb$	$^{206}Pb/^{238}U$	$^{207}Pb/^{235}U$	$^{206}Pb/^{238}U$ age ± 1σ	$^{207}Pb/^{235}U$ age ± 1σ	$^{207}Pb/^{206}Pb$ age ± 1σ
KG1-1	170	134	2546	0.2290 ± 73	0.0674 ± 29	0.1404 ± 20	1.307 ± 61	847 ± 11	849 ± 27	853 ± 89
KG1-2	206	232	11,261	0.3465 ± 49	0.0693 ± 17	0.1395 ± 19	1.333 ± 40	842 ± 11	860 ± 17	908 ± 52
KG1-4	178	184	5914	0.3226 ± 46	0.0682 ± 16	0.1396 ± 19	1.312 ± 37	843 ± 11	851 ± 16	873 ± 48
KG1-5	203	194	2241	0.3028 ± 52	0.0690 ± 19	0.1399 ± 19	1.331 ± 43	844 ± 11	859 ± 19	899 ± 57
KG1-6	164	126	2544	0.2350 ± 56	0.0670 ± 22	0.1399 ± 19	1.294 ± 47	844 ± 11	843 ± 21	839 ± 67
KG1-7	85	103	2961	0.4019 ± 126	0.0702 ± 48	0.1395 ± 21	1.350 ± 97	842 ± 12	867 ± 42	934 ± 141
KG1-8	167	1711	3288	0.3106 ± 59	0.0685 ± 22	0.1402 ± 19	1.324 ± 48	846 ± 11	856 ± 21	883 ± 65
KG2-1	297	234	158	0.2771 ± 151	0.0662 ± 61	0.1135 ± 15	1.035 ± 99	693 ± 9	722 ± 48	812 ± 190
KG2-2	544	361	40,950	0.1988 ± 23	0.0661 ± 8	0.1336 ± 15	1.218 ± 22	808 ± 9	809 ± 10	811 ± 26
KG2-3	705	428	7771	0.1919 ± 24	0.0661 ± 9	0.1201 ± 13	1.096 ± 20	731 ± 8	751 ± 10	811 ± 28
KG2-4	466	290	1204	0.1906 ± 46	0.0662 ± 18	0.1236 ± 14	1.128 ± 35	752 ± 8	767 ± 17	812 ± 57
KG2-5	965	264	1088	0.0875 ± 40	0.0660 ± 17	0.0734 ± 8	0.668 ± 20	456 ± 5	519 ± 12	806 ± 54
KG2-6	221	106	296,736	0.1410 ± 26	0.0661 ± 11	0.1310 ± 15	1.195 ± 25	794 ± 9	798 ± 12	811 ± 33
KG3-1	1052	739	24,038	0.2077 ± 16	0.0581 ± 6	0.0909 ± 12	0.728 ± 13	561 ± 7	555 ± 7	532 ± 21
KG3-2	759	621	6305	0.2481 ± 24	0.0592 ± 8	0.0913 ± 12	0.745 ± 15	563 ± 7	565 ± 9	574 ± 31
KG3-3	737	501	4409	0.1955 ± 23	0.0598 ± 9	0.0915 ± 12	0.755 ± 16	565 ± 7	571 ± 9	597 ± 32
KG3-4	479	281	4114	0.1766 ± 42	0.0601 ± 17	0.0908 ± 12	0.753 ± 24	560 ± 7	570 ± 14	608 ± 59
KG3-5	515	381	5621	0.2346 ± 31	0.0590 ± 11	0.0916 ± 12	0.745 ± 18	565 ± 7	565 ± 10	567 ± 41
KG3-6	358	211	2162	0.2045 ± 61	0.0603 ± 24	0.0906 ± 12	0.753 ± 33	559 ± 7	570 ± 19	613 ± 87
KG5-1	98	122	3839	0.3734 ± 109	0.0683 ± 39	0.1387 ± 21	1.306 ± 80	837 ± 12	849 ± 35	879 ± 119
KG5-2	141	141	2975	0.2932 ± 75	0.0681 ± 27	0.1381 ± 20	1.297 ± 57	834 ± 11	844 ± 25	871 ± 83
KG5-3	173	172	4843	0.3025 ± 59	0.0695 ± 21	0.1375 ± 19	1.317 ± 45	830 ± 11	853 ± 20	913 ± 61
KG5-4	119	168	2000	0.4288 ± 110	0.0679 ± 40	0.1383 ± 20	1.293 ± 81	835 ± 12	843 ± 36	864 ± 122
KG5-5	188	324	7800	0.5160 ± 70	0.0672 ± 19	0.1380 ± 19	1.279 ± 42	833 ± 11	836 ± 19	844 ± 59
KG5-6	138	118	6369	0.2818 ± 85	0.0691 ± 33	0.1375 ± 20	1.310 ± 67	831 ± 11	850 ± 29	902 ± 98
KG5-7	231	266	10,471	0.3488 ± 49	0.0672 ± 16	0.1387 ± 19	1.284 ± 37	837 ± 11	839 ± 17	843 ± 50
KG5-8	175	221	4424	0.3848 ± 58	0.0678 ± 18	0.1380 ± 19	1.290 ± 41	833 ± 11	841 ± 18	863 ± 55
KG11-1	158	165	3899	0.3085 ± 55	0.0664 ± 20	0.1332 ± 15	1.218 ± 41	806 ± 9	809 ± 18	818 ± 62
KG11-2	170	165	11,141	0.2782 ± 43	0.0657 ± 15	0.1344 ± 15	1.217 ± 33	813 ± 9	809 ± 15	796 ± 49
KG11-3	287	214	26,987	0.2271 ± 26	0.0663 ± 9	0.1142 ± 12	1.045 ± 19	697 ± 7	726 ± 10	817 ± 28
KG11-4	512	941	86,851	0.5550 ± 27	0.0655 ± 6	0.1342 ± 15	1.213 ± 18	812 ± 8	806 ± 8	792 ± 18
KG11-5	428	262	40,685	0.1837 ± 19	0.0661 ± 7	0.1338 ± 15	1.219 ± 20	809 ± 8	809 ± 9	809 ± 22
KG33-1	222	178	2972	0.2461 ± 37	0.0651 ± 14	0.1275 ± 10	1.144 ± 28	773 ± 6	774 ± 13	777 ± 46
KG33-2	254	162	8734	0.1894 ± 18	0.0827 ± 7	0.2164 ± 17	2.468 ± 31	1263 ± 9	1263 ± 9	1262 ± 17
KG33-3	888	62	11,173	0.0238 ± 8	0.0686 ± 4	0.1481 ± 12	1.402 ± 15	890 ± 7	890 ± 6	888 ± 12
KG33-4	303	580	4655	0.5773 ± 32	0.0720 ± 9	0.1662 ± 13	1.651 ± 26	991 ± 7	990 ± 10	987 ± 26
KG33-5	771	254	10,695	0.1326 ± 12	0.0659 ± 5	0.1333 ± 10	1.212 ± 14	807 ± 6	806 ± 6	804 ± 15
KG33-6	37	<1	485	0.0087 ± 288	0.0553 ± 120	0.0811 ± 13	0.618 ± 136	503 ± 8	489 ± 86	424 ± 424
KG33-7	274	671	2598	0.7434 ± 63	0.0584 ± 18	0.0899 ± 7	0.724 ± 24	553 ± 4	553 ± 14	546 ± 68
KG36-1	176	108	1801	0.1778 ± 50	0.0659 ± 20	0.1321 ± 11	1.199 ± 40	800 ± 6	800 ± 18	802 ± 65
KG36-2	377	487	1727	0.4162 ± 41	0.0661 ± 15	0.1311 ± 11	1.195 ± 30	794 ± 6	798 ± 14	809 ± 47
KG36-3	290	301	2004	0.3132 ± 41	0.0659 ± 16	0.1320 ± 11	1.199 ± 31	799 ± 6	800 ± 14	803 ± 50
KG36-4	1127	139	655	0.0349 ± 25	0.0800 ± 11	0.2009 ± 16	2.217 ± 36	1180 ± 9	1186 ± 11	1198 ± 26
KG36-5	250	113	2672	0.1466 ± 35	0.0654 ± 14	0.1323 ± 11	1.194 ± 29	801 ± 6	798 ± 13	789 ± 46
KG36-6	186	143	1854	0.2328 ± 50	0.0654 ± 20	0.1320 ± 11	1.190 ± 39	799 ± 6	796 ± 18	786 ± 64
KG37-1	278	181	1625	0.1865 ± 57	0.0563 ± 23	0.0760 ± 6	0.590 ± 25	472 ± 4	471 ± 16	463 ± 89
KG37-2	100	38	1334	0.1321 ± 106	0.0567 ± 43	0.0761 ± 7	0.596 ± 46	473 ± 4	474 ± 30	481 ± 169
KG37-3	229	139	7593	0.1922 ± 34	0.0565 ± 12	0.0759 ± 6	0.592 ± 14	472 ± 4	472 ± 9	474 ± 47
KG37-4	94	101	1616	0.3387 ± 83	0.0652 ± 32	0.1291 ± 12	1.161 ± 59	783 ± 7	782 ± 28	782 ± 102
KG37-5	286	176	3591	0.1855 ± 41	0.0567 ± 16	0.0758 ± 6	0.593 ± 18	471 ± 4	473 ± 11	480 ± 61
KG38-1	184	97	1709	0.1648 ± 67	0.0575 ± 27	0.0759 ± 6	0.602 ± 29	472 ± 4	479 ± 18	512 ± 102
KG38-2	265	158	1778	0.1907 ± 46	0.0573 ± 18	0.0758 ± 6	0.599 ± 20	471 ± 4	477 ± 13	502 ± 68
KG38-3	193	134	1715	0.2187 ± 70	0.0565 ± 28	0.0761 ± 6	0.593 ± 30	473 ± 4	473 ± 19	474 ± 108
KG38-4	239	177	10,091	0.2245 ± 33	0.0566 ± 11	0.0761 ± 6	0.594 ± 13	473 ± 4	473 ± 8	474 ± 43
KG38-5	95	301	1069	0.0688 ± 123	0.0568 ± 51	0.0758 ± 7	0.594 ± 54	471 ± 4	473 ± 35	483 ± 199
KG39-1	491	260	4522	0.1729 ± 28	0.0584 ± 11	0.0874 ± 7	0.703 ± 15	540 ± 4	541 ± 9	544 ± 41
KG39-2	392	255	4129	0.2086 ± 31	0.0587 ± 11	0.0874 ± 7	0.707 ± 16	540 ± 4	543 ± 9	556 ± 43
KG39-3	356	228	3405	0.1994 ± 34	0.0584 ± 13	0.0875 ± 7	0.704 ± 18	541 ± 4	541 ± 10	544 ± 49
KG39-4	163	95	2012	0.1866 ± 64	0.0585 ± 26	0.0876 ± 7	0.707 ± 32	542 ± 4	543 ± 19	549 ± 95
KG39-5	477	278	4195	0.1816 ± 27	0.0588 ± 10	0.0876 ± 7	0.711 ± 14	542 ± 4	545 ± 8	560 ± 38
KG39-6	654	527	6671	0.2444 ± 20	0.0583 ± 7	0.0875 ± 7	0.704 ± 11	541 ± 4	541 ± 6	541 ± 27
KG42-1	423	395	75,188	0.2966 ± 34	0.0528 ± 10	0.0508 ± 9	0.370 ± 10	320 ± 6	320 ± 8	319 ± 44
KG42-2	1267	2911	21,820	0.7199 ± 29	0.0528 ± 5	0.0512 ± 9	0.372 ± 8	322 ± 6	321 ± 6	320 ± 20
KG42-3	613	959	17,841	0.5084 ± 32	0.0532 ± 7	0.0512 ± 9	0.376 ± 9	322 ± 6	324 ± 6	337 ± 27
KG42-4	735	1216	12,297	0.5108 ± 33	0.0532 ± 7	0.0513 ± 9	0.376 ± 9	322 ± 6	324 ± 7	337 ± 29
KG42-5	793	1272	20,096	0.5101 ± 29	0.0532 ± 6	0.0507 ± 9	0.372 ± 8	319 ± 6	321 ± 6	338 ± 24
KG42-6	504	785	11,001	0.5004 ± 45	0.0536 ± 10	0.0509 ± 9	0.376 ± 10	320 ± 6	324 ± 8	354 ± 43
KG42-7	606	926	6169	0.4792 ± 40	0.0532 ± 9	0.0512 ± 9	0.376 ± 11	322 ± 6	324 ± 7	339 ± 40
KG42-8	925	1478	9424	0.4965 ± 48	0.0528 ± 11	0.0515 ± 9	0.375 ± 11	324 ± 6	324 ± 8	322 ± 47
KG42-9	608	1022	15,632	0.5460 ± 35	0.0531 ± 7	0.0506 ± 9	0.370 ± 9	318 ± 6	320 ± 7	333 ± 30
KG42-10	552	753	9949	0.4327 ± 32	0.0530 ± 7	0.0509 ± 9	0.372 ± 9	320 ± 6	321 ± 7	331 ± 32
KG42-11	983	2211	22,467	0.6871 ± 32	0.0529 ± 5	0.0510 ± 9	0.371 ± 8	320 ± 6	321 ± 6	324 ± 23
KG42-12	494	747	7733	0.4952 ± 47	0.0533 ± 10	0.0513 ± 9	0.377 ± 11	322 ± 6	325 ± 8	343 ± 44

Table 3 (*continued*)

Sample #*	U ppm	Th ppm	$^{206}Pb/^{204}Pb$	$^{208}Pb/^{206}Pb$	$^{207}Pb/^{206}Pb$	$^{206}Pb/^{238}U$	$^{207}Pb/^{235}U$	$^{206}Pb/^{238}U$ age ± 1σ	$^{207}Pb/^{235}U$ age ± 1σ	$^{207}Pb/^{206}Pb$ age ± 1σ
KG43-1	130	168	49,116	0.3982 ± 42	0.0665 ± 10	0.1349 ± 10	1.237 ± 21	816 ± 6	817 ± 10	821 ± 31
KG43-2	177	145	48,972	0.2458 ± 31	0.0664 ± 10	0.1350 ± 10	1.236 ± 21	816 ± 6	816 ± 10	819 ± 31
KG43-3	131	116	3364	0.2584 ± 50	0.0666 ± 18	0.1343 ± 10	1.234 ± 36	813 ± 6	816 ± 17	826 ± 58
KG43-4	165	227	4521	0.4106 ± 47	0.0662 ± 14	0.1344 ± 10	1.227 ± 29	813 ± 6	813 ± 13	812 ± 45
KG43-5	172	121	3849	0.2028 ± 40	0.0665 ± 15	0.1345 ± 10	1.234 ± 31	814 ± 6	816 ± 14	822 ± 48
KG44-1	3251	3333	24,067	0.3293 ± 9	0.0557 ± 2	0.0722 ± 13	0.555 ± 10	449 ± 8	448 ± 7	442 ± 9
KG44-2	4722	4266	1639	0.2797 ± 10	0.0561 ± 4	0.0612 ± 11	0.473 ± 9	383 ± 7	393 ± 6	458 ± 14
KG44-3	4229	4522	17,553	0.2164 ± 9	0.0561 ± 3	0.0724 ± 13	0.560 ± 11	451 ± 8	452 ± 7	458 ± 11
KG44-4	1982	1436	68,120	0.2689 ± 8	0.0561 ± 2	0.0712 ± 13	0.551 ± 10	443 ± 8	446 ± 7	456 ± 8
KG44-5	3161	2894	9626	0.2550 ± 13	0.0559 ± 4	0.0725 ± 13	0.559 ± 11	451 ± 8	451 ± 7	450 ± 16
KG44-6	1917	1617	3989	0.1972 ± 12	0.0562 ± 4	0.0719 ± 13	0.557 ± 11	448 ± 8	450 ± 7	460 ± 18
KG44-7	1656	1025	101,937	0.3676 ± 10	0.0558 ± 2	0.0726 ± 13	0.558 ± 11	452 ± 8	450 ± 7	443 ± 9
KG44-8	1906	1037	1907	0.4083 ± 11	0.0562 ± 3	0.0652 ± 12	0.505 ± 10	407 ± 7	415 ± 7	459 ± 13
KG44-9	3176	3725	9403	0.1779 ± 6	0.0560 ± 2	0.0430 ± 8	0.332 ± 6	272 ± 5	291 ± 5	452 ± 9
KG44-10	7713	10,618	30,488	0.1124 ± 4	0.0562 ± 2	0.0677 ± 12	0.525 ± 1^0	423 ± 7	428 ± 7	459 ± 7
KG46-1	529	28	10,324	0.0163 ± 13	0.0592 ± 6	0.0943 ± 6	0.770 ± 99	581 ± 4	579 ± 6	575 ± 22
KG46-2	386	320	2921	0.2524 ± 30	0.0643 ± 11	0.1281 ± 9	1.136 ± 23	777 ± 5	771 ± 11	752 ± 38
KG46-3	512	362	299	0.2709 ± 81	0.0650 ± 33	0.1284 ± 10	1.152 ± 60	779 ± 6	778 ± 28	776 ± 107
KG46-4	306	300	9183	0.2972 ± 23	0.0649 ± 8	0.1284 ± 9	1.149 ± 16	779 ± 5	777 ± 8	772 ± 25
KG46-5	173	108	4507	0.1789 ± 33	0.0648 ± 13	0.1283 ± 9	1.146 ± 25	778 ± 5	775 ± 12	768 ± 42
KG47-1	55	46	454	0.2526 ± 251	0.0577 ± 101	0.0860 ± 12	0.684 ± 122	532 ± 8	529 ± 74	518 ± 394
KG47-2	44	26	623	0.2531 ± 315	0.0579 ± 128	0.0862 ± 15	0.687 ± 154	533 ± 9	531 ± 93	524 ± 473
KG47-3	64	34	527	0.1674 ± 232	0.0598 ± 95	0.0859 ± 12	0.708 ± 114	531 ± 7	544 ± 68	597 ± 350
KG47-4	123	158	1284	0.3947 ± 106	0.0598 ± 40	0.0856 ± 9	0.706 ± 49	529 ± 5	542 ± 29	597 ± 146
KG47-5	110	133	1418	0.3865 ± 106	0.0596 ± 40	0.0860 ± 9	0.706 ± 49	532 ± 5	543 ± 29	588 ± 145
KG47-6	71	68	491	0.2939 ± 218	0.0570 ± 88	0.0859 ± 12	0.675 ± 106	531 ± 7	524 ± 64	490 ± 346
KG47-7	42	25	934	0.1642 ± 169	0.0570 ± 69	0.0859 ± 10	0.675 ± 83	532 ± 6	524 ± 50	490 ± 269
KG49-1	295	139	2522	0.1349 ± 42	0.0553 ± 17	0.0727 ± 7	0.555 ± 18	453 ± 4	448 ± 12	425 ± 69
KG49-2	348	246	3643	0.2118 ± 33	0.0570 ± 13	0.0726 ± 6	0.570 ± 14	452 ± 4	458 ± 9	490 ± 49
KG49-3	516	456	5079	0.2665 ± 27	0.0551 ± 10	0.0728 ± 6	0.553 ± 12	453 ± 4	447 ± 8	415 ± 41
KG49-4	1380	1267	455	0.2786 ± 42	0.0560 ± 17	0.0724 ± 7	0.559 ± 18	451 ± 4	451 ± 12	453 ± 66
KG49-5	638	493	631	0.2426 ± 63	0.0558 ± 25	0.0728 ± 6	0.559 ± 26	453 ± 3	451 ± 17	442 ± 101
KG49-6	618	308	6301	0.1670 ± 22	0.0559 ± 8	0.0727 ± 5	0.560 ± 10	452 ± 3	452 ± 6	447 ± 34

* KG1-1 is spot on grain 1; KG1-2 is spot on grain 2, etc.

Sample KG 2 is a slightly migmatitic red granite-gneiss (Fig. 12a), collected on the road to Chon–Kemin some 1 km E of KG 1 (Table 1, Fig. 2) but does not exhibit finely layered texture as in KG 1. The sample consists of quartz, microcline, strongly seriticized plagioclase and well aligned muscovite and biotite. Biotite is partly chloritized, and larger quartz grains are fragmented, and the aggregates are aligned in the foliation. The zircons, as in previous samples, are euhedral and stubby to long-prismatic with partly rounded terminations. Cl-images show well developed oscillatory magmatic zoning (Fig. 11b, inset). Six grains were analyzed, and in contrast to the previous samples, most zircons experienced variable recent Pb-loss and thus define a discordia line (MSWD = 0.01) intersecting Concordia at 811 ± 28 Ma (Fig. 11b). The five least discordant analyses define a mean $^{207}Pb/^{206}Pb$ age of 810 ± 4.2 Ma, which we consider to most closely reflect the time of gneiss protolith emplacement. The large error in the intercept age makes this rock time-equivalent with KG 1, but the mean $^{207}Pb/^{206}Pb$ age suggests it to be slightly younger, in line with the suggested field relationship. The $\varepsilon_{Nd(t)}$ value for whole-rock sample KG 2 is −11.8, and the corresponding mean crustal residence age is 1.80 Ga (Table 5), similar to sample KG 1. Clearly, the gneiss protolith is a crustal-melt granite, and both gneiss precursors were most likely derived from broadly the same crustal source.

Sample KG 11 is a granodioritic gneiss, similar in appearance to KG 1 and displays strong ductile deformation. It was collected near the Bishkek–Naryn road close to the Chu River (Table 1, Fig. 2) and contains a large boudin of amphibolite (Fig. 12b), which we interpret to be a remnant of the same dyke system as exposed at Aktyuz village. The relatively coarse-grained rock is composed of quartz, slight to severely seriticized plagioclase, large poikilitic hornblende, and a little orthoclase. The zircons are mostly long-prismatic and show significant rounding at their ends. Striped oscillatory zoning is common in many grains (Fig. 11c, inset). Analysis of five grains (Table 3) produced four concordant and well-grouped results with a mean $^{206}Pb/^{238}U$ age of 810 ± 10 Ma (Fig. 11c). One analysis is grossly discordant due to Recent Pb-loss and is not considered for age assessment. The above age, interpreted to reflect protolith emplacement, is identical to the $^{207}Pb/^{206}Pb$ age of sample KG 2 and confirms the Early Neoproterozoic origin of the granitoid complex that was to become the Kemin Complex.

The $\varepsilon_{Nd(t)}$ value for whole-rock sample KG 11 is strongly negative at −12.3, and the corresponding mean crustal residence age is 2.11 Ga (Table 5), similar to KG 1 and the oldest in our study. As with all other samples discussed so far the gneiss protolith was a crustal-melt granodiorite, and it is most likely that both KG 1 and KG 11 gneiss precursors were derived from similar crustal sources.

Sample KG 33 is a strongly foliated migmatitic "granitic-looking" paragneiss of the Kemin Complex collected in the Taldybulak River valley south of Orlovka village (Table 1, Fig. 2). In this gneiss, presumably derived from arkosic sediment, the colourless to dark red-brown detrital zircon population is heterogeneous and variably but generally well rounded. Under CL most grains have dark, U-rich cores rimmed by high-luminescence (U-poor) zones which probably reflect metamorphic overgrowth but were too narrow for SHRIMP analysis (Fig. 11d, inset). Seven grains were analyzed on SHRIMP II, and all results are concordant (Table 3) and display an age range from 503 to 1263 Ma (Fig. 11d). As is often the case with detrital zircons, the two least rounded grains are the youngest, whereas the well-rounded grains are significantly older. Although the number of analyses is insufficient to make any meaningful assumption as to the source area

Table 4
Lu–Hf isotopic data of zircons from samples KG 1 and KG 5, Kyrgyz northern Tianshan.

Spot	$^{176}Yb/^{177}Hf$	±(2σ)	$^{176}Lu/^{177}Hf$	±(2σ)	$^{176}Hf/^{177}Hf$	±(2σ)	t (Ma)	$(^{176}Hf/^{177}Hf)_i$	$\varepsilon_{Hf}(t)$	±(1σ)	t_{DM} (Ga)	±(1σ)	*tc* (Ga)*	±(1σ)	*tc* (Ga)†	±(1σ)
KG1-1	0.032824	0.000387	0.001451	0.000021	0.281760	0.000027	844	0.281737	−18.00	0.48	2.12	0.02	2.53	0.02	2.88	0.03
KG1-2	0.029723	0.001020	0.001317	0.000043	0.281802	0.000041	844	0.281781	−16.45	0.72	2.05	0.03	2.45	0.04	2.78	0.05
KG1-3	0.037750	0.000667	0.001694	0.000028	0.281723	0.000034	844	0.281696	−19.45	0.59	2.19	0.02	2.60	0.03	2.97	0.04
KG1-4	0.025281	0.001890	0.001100	0.000076	0.281740	0.000123	844	0.281722	−18.52	2.15	2.13	0.08	2.55	0.11	2.91	0.14
KG1-5	0.051037	0.001450	0.002225	0.000058	0.281769	0.000044	844	0.281733	−18.14	0.78	2.15	0.03	2.53	0.04	2.89	0.05
KG1-6	0.033887	0.000763	0.001504	0.000032	0.281727	0.000044	844	0.281704	−19.19	0.76	2.17	0.03	2.59	0.04	2.95	0.05
KG1-7	0.024410	0.000584	0.001062	0.000030	0.281771	0.000046	844	0.281754	−17.41	0.80	2.08	0.03	2.49	0.04	2.84	0.05
KG1-8	0.025145	0.001230	0.001112	0.000050	0.281782	0.000045	844	0.281764	−17.04	0.79	2.07	0.03	2.48	0.04	2.82	0.05
KG1-9	0.022853	0.001770	0.001040	0.000081	0.281766	0.000055	844	0.281750	−17.55	0.97	2.09	0.04	2.50	0.05	2.85	0.06
KG1-10	0.018994	0.000380	0.000835	0.000018	0.281816	0.000052	844	0.281803	−15.67	0.92	2.01	0.04	2.40	0.05	2.73	0.06
KG5-1	0.025015	0.000741	0.001118	0.000031	0.282020	0.000038	834	0.282003	−8.82	0.66	1.74	0.03	2.04	0.03	2.30	0.04
KG5-2	0.027386	0.001000	0.001186	0.000041	0.282195	0.000033	834	0.282176	−2.66	0.57	1.50	0.02	1.72	0.03	1.91	0.04
KG5-3	0.020785	0.000104	0.000912	0.000004	0.282082	0.000035	834	0.282067	−6.53	0.61	1.65	0.02	1.92	0.03	2.15	0.04
KG5-4	0.090952	0.001030	0.003692	0.000034	0.281908	0.000028	834	0.281850	−14.24	0.48	2.03	0.02	2.32	0.03	2.64	0.03
KG5-5	0.038553	0.001020	0.001672	0.000039	0.282105	0.000035	834	0.282079	−6.11	0.62	1.65	0.02	1.90	0.03	2.12	0.04
KG5-6	0.038167	0.002040	0.001661	0.000074	0.282141	0.000039	834	0.282115	−4.86	0.68	1.60	0.03	1.83	0.04	2.05	0.04
KG5-7	0.026702	0.000211	0.001170	0.000010	0.282067	0.000026	834	0.282049	−7.18	0.45	1.68	0.02	1.96	0.02	2.19	0.03
KG5-8	0.017311	0.000224	0.000763	0.000010	0.282035	0.000034	834	0.282023	−8.10	0.59	1.70	0.02	2.00	0.03	2.25	0.04
KG5-9	0.026109	0.000180	0.001154	0.000006	0.282162	0.000025	834	0.282144	−3.82	0.44	1.54	0.02	1.78	0.02	1.98	0.03
KG5-10	0.032973	0.001380	0.001465	0.000064	0.282128	0.000034	834	0.282105	−5.19	0.60	1.60	0.02	1.85	0.03	2.07	0.04
KG5-11	0.031711	0.001540	0.001398	0.000062	0.282178	0.000037	834	0.282157	−3.37	0.64	1.53	0.03	1.76	0.03	1.95	0.04
KG5-12	0.026615	0.000258	0.001164	0.000013	0.282109	0.000032	834	0.282091	−5.70	0.57	1.62	0.02	1.88	0.03	2.10	0.04
KG5-13	0.086929	0.000628	0.003542	0.000022	0.282020	0.000019	834	0.281965	−10.15	0.34	1.86	0.01	2.11	0.02	2.38	0.02
KG5-14	0.026068	0.000393	0.001132	0.000016	0.282149	0.000034	834	0.282131	−4.28	0.60	1.56	0.02	1.80	0.03	2.01	0.04
KG5-15	0.023016	0.000222	0.001006	0.000009	0.282137	0.000019	834	0.282121	−4.62	0.34	1.57	0.01	1.82	0.02	2.03	0.02
KG5-16	0.028322	0.000528	0.001272	0.000020	0.282048	0.000050	834	0.282028	−7.92	0.88	1.71	0.03	1.99	0.05	2.24	0.06
KG5-17	0.026885	0.000616	0.001155	0.000025	0.282111	0.000048	834	0.282092	−5.64	0.85	1.62	0.03	1.87	0.04	2.09	0.05
KG5-18	0.025771	0.000251	0.001133	0.000009	0.282073	0.000045	834	0.282055	−6.96	0.78	1.67	0.03	1.94	0.04	2.18	0.05
KG5-19	0.036129	0.001090	0.001526	0.000045	0.282178	0.000029	834	0.282154	−3.47	0.51	1.54	0.02	1.76	0.03	1.96	0.03
KG5-20	0.030900	0.000755	0.001264	0.000040	0.281837	0.000075	834	0.281817	−15.40	1.30	2.00	0.05	2.38	0.07	2.71	0.08
KG5-21	0.029416	0.000790	0.001300	0.000036	0.282063	0.000063	834	0.282043	−7.40	1.11	1.69	0.04	1.97	0.06	2.21	0.07
KG5-22	0.032355	0.001190	0.001380	0.000046	0.282079	0.000039	834	0.282058	−6.87	0.69	1.67	0.03	1.94	0.04	2.17	0.04
KG5-23	0.035426	0.002230	0.001538	0.000089	0.282204	0.000065	834	0.282179	−2.56	1.13	1.50	0.05	1.71	0.06	1.90	0.07
KG5-24	0.042163	0.002190	0.001802	0.000090	0.282143	0.000052	834	0.282115	−4.83	0.92	1.60	0.04	1.83	0.05	2.04	0.06
KG5-25	0.029067	0.001100	0.001283	0.000045	0.282077	0.000036	834	0.282056	−6.91	0.63	1.67	0.03	1.94	0.03	2.18	0.04
KG5-26	0.030114	0.000412	0.001332	0.000018	0.282112	0.000049	834	0.282091	−5.69	0.86	1.62	0.03	1.88	0.05	2.10	0.06
KG5-27	0.035017	0.002180	0.001524	0.000086	0.282130	0.000067	834	0.282106	−5.15	1.18	1.60	0.05	1.85	0.06	2.06	0.08
KG5-28	0.048082	0.002040	0.001977	0.000078	0.282127	0.000045	834	0.282096	−5.50	0.78	1.63	0.03	1.87	0.04	2.09	0.05
KG5-29	0.029072	0.000330	0.001274	0.000015	0.282094	0.000047	834	0.282074	−6.30	0.82	1.64	0.03	1.91	0.04	2.14	0.05

* Crustal age is calculated using $^{176}Lu/^{177}Hf = 0.010$.
† Crustal age is calculated using $^{176}Lu/^{177}Hf = 0.015$.

of the Kemin paragneiss, it is obvious that the metamorphic event that transformed the original metasediment into a migmatitic gneiss must be younger than 503 ± 8 Ma. By implication, migmatization in both the Aktyuz and Kemin Complexes was probably Early Palaeozoic in age.

Sample KG 36 is a layered migmatitic granite-gneiss (Fig. 13a) of the Kokbulak migmatite suite of Bakirov et al. (2003). The dated sample is predominantly granitic in composition and does not display palaeosome and neosome veins as usually found in migmatites. We therefore prefer to interpret this rock as a strongly deformed granite-

Table 5
Sm–Nd isotopic data for granitoid rocks and an eclogite sample from the Kemin–Aktyuz and Dolpran Complexes, northern Tianshan, Kyrgyzstan*.

Sample	Age [Ma]	Rock type	Sm [μg/g]	Nd [μg/g]	$^{147}Sm/^{144}Nd$	$^{143}Nd/^{144}Nd$ (m.)	$\varepsilon_{Nd(t)}$	t_{DM}
Kemin Complex								
KG 1	844	Granite gneiss	5.875	34.76	0.1022	0.511543 ± 10	−11.2	2.04
KG 2	810	Granite-gneiss	4.829	29.87	0.09773	0.511668 ± 10	−11.8	1.80
KG 11	810	Tonalitic gneiss	5.100	29.64	0.1040	0.511514 ± 8	−12.3	2.11
Aktyuz Complex								
KG 3	562	Granite gneiss	10.25	50.77	0.1220	0.512115 ± 8	−4.8	1.53
KG 5	834	Orthogneiss	4.791	28.77	0.1007	0.511872 ± 11	−4.7	1.57
KG 8	600(?)	Eclogite	3.533	12.87	0.1659	0.512708 ± 10	3.7	–
Dolpran Complex								
KG 37	472	Granodiorite	2.231	10.63	0.1269	0.512297 ± 10	−2.5	1.30
KG 38	472	Granodiorite	2.814	12.43	0.1369	0.512357 ± 9	−1.9	1.35

External precision for $^{143}Nd/^{144}Nd$ is ~1.1×10^{-5} (2 SD). Error for $^{147}Sm/^{144}Nd$ ~0.2% (2 SD). Sm and Nd concentrations determined by isotope dilution, m. = measured ratio, t = initial ratio. Model age calculation according to DePaolo (1988).
* $^{143}Nd/^{144}Nd$ normalized to $^{146}Nd/^{144}Nd = 0.7219$.

Table 6
Laser $^{40}Ar/^{39}Ar$ analytical data for two muscovite grains from gneiss samples KG 40 and KG 46.

Sample	Lab no.	Laser power (mV)	^{40}Ar (mol)	^{40}Ar (V)	±1σ	^{39}Ar (V)	±1σ	^{38}Ar (V)	±1σ	^{37}Ar (V)	±1σ	^{36}Ar (V)	±1σ	$^{40}Ar^*/^{39}Ar$	±1σ	% $^{40}Ar^*$	Age (Ma)	±2σ
KG40	B399-1	–	–	0.001855	0.000089	0.000093	0.000013	0.000011	0.000004	0.000048	0.000005	0.000021	0.000006	–	–	–	–	–
Muscovite	K399-1	400	1.914E-15	0.097539	0.000083	0.005871	0.000031	0.000083	0.000004	0.000047	0.000006	0.000039	0.000004	15.602607	0.39808	94.24	477.10	±21.39
	K399-2	438	5.889E-15	0.296325	0.000515	0.018568	0.000068	0.000247	0.000006	0.000038	0.000007	0.000039	0.000007	15.618410	0.22034	98.01	477.52	±11.84
	K399-3	460	1.886E-14	0.944745	0.001562	0.060694	0.000146	0.000748	0.000012	0.000020	0.000008	0.000017	0.000008	15.546458	0.16875	99.94	475.59	±9.08
	B399-2	–	–	0.001800	0.000067	0.000077	0.000009	0.000010	0.000003	0.000060	0.000006	0.000036	0.000006	–	–	–	–	–
	K399-4	480	4.849E-14	2.426077	0.005846	0.158292	0.000390	0.001939	0.000019	0.000012	0.000009	0.000017	0.000016	15.326566	0.16533	100.04	469.67	±8.92
	K399-5	500	2.997E-14	1.500304	0.002565	0.097550	0.000157	0.001189	0.000010	0.000021	0.000011	0.000017	0.000010	15.400182	0.16227	100.19	471.65	±8.75
	K399-6	530	5.857E-14	2.930223	0.004265	0.190942	0.000435	0.002361	0.000013	0.000031	0.000015	0.000017	0.000013	15.340730	0.16048	100.01	470.05	± 8.66
	B399-3	–	–	0.000028	0.000005	0.000068	0.000004	0.000015	0.000003	0.000173	0.000019	0.002969	0.000197	–	–	–	–	–
	K399-7	570	4.468E-14	2.236719	0.004530	0.145891	0.000325	0.001770	0.000019	0.000009	0.000009	0.000033	0.000041	15.284937	0.18104	99.73	468.54	±9.77
	K399-8	620	3.779E-14	1.892366	0.003191	0.123166	0.000211	0.001516	0.000014	0.000033	0.000016	0.000011	0.000011	15.369468	0.16087	100.07	470.82	±8.68
	K399-9	680	2.997E-14	1.501586	0.002439	0.097896	0.000123	0.001171	0.000016	0.000019	0.000005	0.000001	0.000007	15.382092	0.15934	100.32	471.17	±8.59
	K399-10	999	3.286E-14	1.646139	0.002040	0.106896	0.000169	0.001301	0.000010	0.000083	0.000011	0.000015	0.000023	15.399376	0.17037	100.04	471.63	±9.18
KG46	B400-1	–	–	0.002932	0.000154	0.000135	0.000012	0.000014	0.000005	0.000060	0.000006	0.000044	0.000006	–	–	–	–	–
Muscovite	K400-1	415	1.417E-18	0.073773	0.000040	0.004071	0.000038	0.000078	0.000004	0.000057	0.000006	0.000083	0.000006	15.150484	0.64622	83.67	464.82	±34.96
	K400-2	460	9.320E-18	0.468911	0.001346	0.024424	0.000064	0.000405	0.000005	0.000040	0.000006	0.000331	0.000007	15.816677	0.27056	81.94	482.75	±14.49
	K400-3	480	1.488E-17	0.746709	0.001250	0.043470	0.000053	0.000601	0.000009	0.000061	0.000005	0.000212	0.000006	16.106213	0.17964	93.27	490.49	±9.58
	B400-2	–	–	0.001316	0.000033	0.000031	0.000005	0.000014	0.000004	0.000058	0.000004	0.000033	0.000005	–	–	–	–	–
	K400-4	510	7.265E-18	0.364578	0.000780	0.023150	0.000048	0.000294	0.000007	0.000039	0.000008	0.000013	0.000007	16.023647	0.19791	101.36	488.29	±10.57
	K400-5	543	1.574E-17	0.788538	0.001405	0.050072	0.000140	0.000618	0.000011	0.000048	0.000009	0.000033	0.000007	15.796351	0.17382	99.80	482.21	±9.31
	K400-6	550	1.159E-16	5.795737	0.011283	0.374058	0.000609	0.004656	0.000026	0.000007	0.000015	0.000007	0.000005	15.577847	0.16082	99.94	476.35	±8.64
	B400-3	–	–	0.004160	0.000322	0.000221	0.000028	0.000006	0.000004	0.000056	0.000004	0.000026	0.000004	–	–	–	–	–
	K400-7	560	9.147E-17	4.577572	0.008621	0.297210	0.000645	0.003641	0.000030	0.000018	0.000036	0.000075	0.000007	15.563567	0.16218	100.45	475.96	± 8.72
	K400-8	600	7.179E-17	3.593799	0.005487	0.233852	0.000378	0.002902	0.000013	0.000004	0.000005	0.000032	0.000011	15.501617	0.15948	100.27	474.30	±8.58
	K400-9	650	3.864E-17	1.936249	0.003043	0.125522	0.000303	0.001545	0.000023	0.000035	0.000007	0.000016	0.000022	15.508024	0.16966	99.96	474.47	±9.13
	B400-4	–	–	0.002753	0.000144	0.000125	0.000015	0.000011	0.000005	0.000060	0.000006	0.000033	0.000006	–	–	–	–	–
	K400-10	725	4.138E-17	2.073276	0.004360	0.134982	0.000297	0.001671	0.000015	0.000015	0.000006	0.000004	0.000009	15.465933	0.16319	100.11	473.34	±8.79
	K400-11	999	1.360E-17	0.682905	0.001257	0.043934	0.000112	0.000553	0.000009	0.000032	0.000010	0.000014	0.000007	15.721068	0.17623	100.64	480.19	±9.45

Samples were irradiated for 30 h with Cd shielding in 5C position at McMaster Nuclear Reactor along with Hb3gr hornblende monitor (1072 Ma; Turner et al., 1971).
J-values range from 0.0035309 ± 0.0000177 (= 0.5% at 1 s) to 0.0035312 ± 0.0000177 (= 0.5% at 1 s).
Data are presented following Renne et al. (2009) recommendations and calculations are determined by using the ArArCALC-software of Koppers (2002).

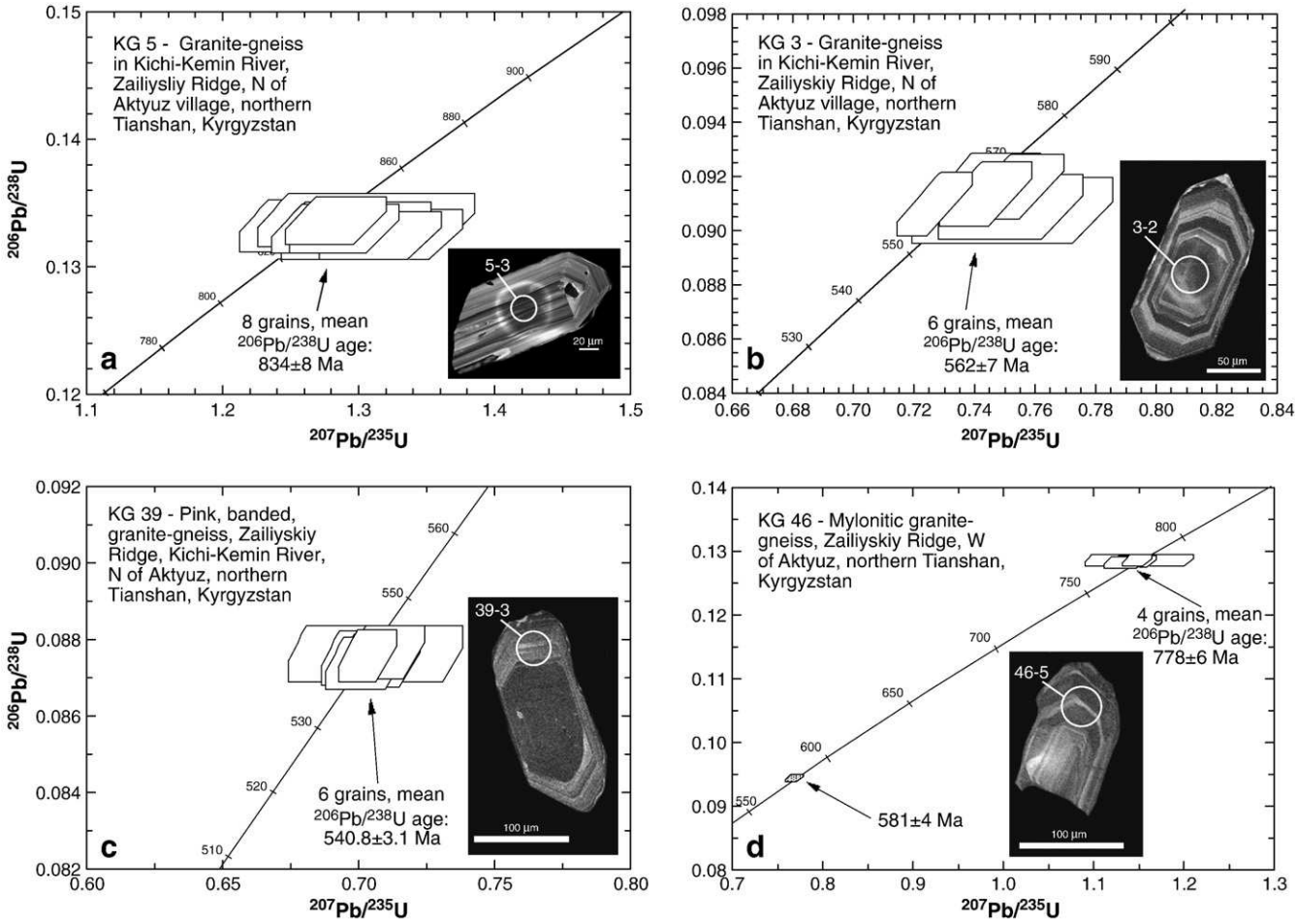

Fig. 7. Concordia diagrams showing analytical data for zircons from granitoid gneisses of the Aktyuz Complex. See Table 3 for details. Data boxes for each analysis are defined by standard errors in $^{207}Pb/^{235}U$ $^{206}Pb/^{238}U$ and $^{207}Pb/^{206}Pb$. Insets show cathodoluminescence images of typical zircon from each sample with number of analysis and white scale bar.

gneiss. The zircons are uniformly long-prismatic with well rounded terminations and well developed oscillatory zoning under CL (Fig. 18a, inset), and some dark cores are visibly metamict. Six typical magmatic grains were analyzed on SHRIMP II (Table 3), and five grains yielded concordant and well grouped results with a mean $^{206}Pb/^{238}U$ age of 799 ± 6 Ma, whereas one morphologically identical grain is much older at 1180 ± 9 Ma (Fig. 14a) and is interpreted as a xenocryst. This age is similar to Neoproterozoic ages reported from the Kemin Complex above, and the homogeneous morphology and internal structure of the zircons confirm our interpretation that this rock is derived from a granitic protolith.

Sample KG 43 is a grey, well-layered and intensely deformed granitic gneiss (Fig. 13b) that was collected at a blasted roadcut on the road along the Chon–Kemin River (Table 1, Fig. 2). The zircons vary in

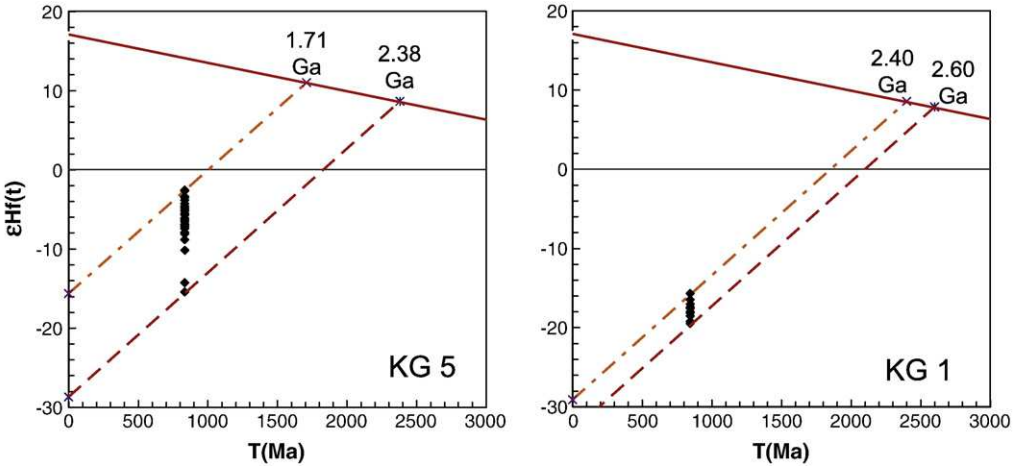

Fig. 8. Hf isotope evolution diagram for zircons from samples KG 5 (left) and KG 1 (right), based on the analytical data of Table 4 and an assumed crustal $^{176}Lu/^{177}Hf$ ratio of 0.010. For explanation see text.

Fig. 9. Strongly sheared and retrogressed granite-gneiss KG 46 of the Aktyuz Complex.

shape from stubby to long-prismatic and, as in previous samples, show slightly to well rounded terminations. Superb oscillatory zoning is ubiquitous under CL (Fig. 14b, inset) Analysis of five grains yielded concordant and well-grouped results (Table 3) with a mean $^{206}Pb/^{238}U$ age of 814 ± 5 Ma (Fig. 14b), which we interpret to represent the time of emplacement of the gneiss protolith. This age is again similar to the protolith ages from the other granitoid gneisses of the Kemin and Aktyuz Complexes. V. Kisilev (pers. comm.) obtained a discordant multigrain zircon population suggesting an age of ca. 1100 Ma from this locality.

4.2.3. Kopurelisai ophiolite suite

The only datable rock in this presumed ophiolitic sequence is an isotropic leucogabbro exposed along the road to Aktyuz (Table 1, Fig. 2). Our sample KG 47 is a strongly foliated and lineated rock representing a large body of massive metagabbro. The zircons are irregular in shape and vary from long-prismatic to oval, but longish grains predominate and are commonly rounded at their terminations. CL images are strongly luminescent showing the low U-content of the zircons, and internal structures are diffuse, but oscillatory and hour-glass zoning can be recognized (Fig. 18c, inset). Seven grains analyzed on SHRIMP II produced concordant and well-grouped results with a mean $^{206}Pb/^{238}U$ age of 531.2 ± 3.7 Ma (Fig. 14c). We interpret this to reflect the time of crystallization of the gabbro and, by implication, the formation age of oceanic crust, if the ophiolitic interpretation of this rock is correct.

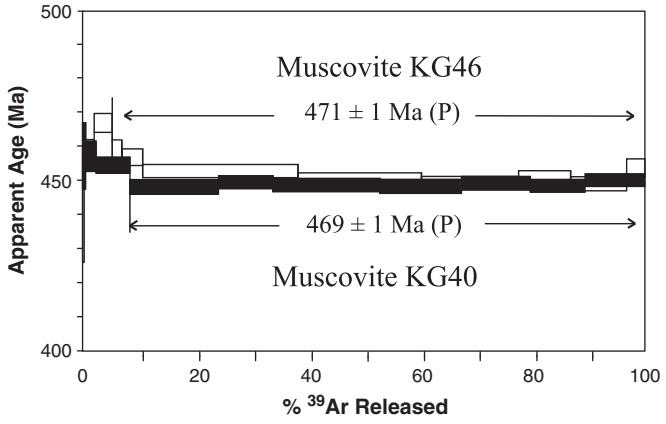

Fig. 10. $^{40}Ar–^{39}Ar$ age spectra as a function of ^{39}Ar released for 2 muscovite grains from granitic gneiss samples KG 40 (black rectangles) and KG 46 (open rectangles). Error boxes for each step are at the 2 σ level. Errors for plateau ages (P) are given at the 2 σ level. The MSWD for plateaux and percentage of ^{39}Ar degassed used in the plateau calculations are listed in Table 6.

4.2.4. Post-kinematic igneous rocks

Finally, we report ages for post-kinematic igneous rocks that have not experienced the pervasive deformation and metamorphism of rocks from the Aktyuz and Kemin Complexes. The Dolpran quartz-diorite, exposed northeast of the village of Ilyich (Fig. 2), is a relatively homogeneous pluton, locally deformed into a streaky hornblende gneiss and occasionally containing stretched xenoliths of gabbro (Fig. 15a), presumably derived from early phase of the pluton. Much of the pluton is a completely undeformed, coarse-grained quartz-diorite (Fig. 15b).

The zircons in sample KG 37 are predominantly idiomorphic and long-prismatic with no rounding at their terminations and show excellent oscillatory zoning under CL (Fig. 16a, inset). Five grains were analyzed on SHRIMP II (Table 3). Four analyses are virtually identical and define a concordant group with a mean $^{206}Pb/^{238}U$ age of 471.9 ± 3.5 Ma (Fig. 16a). One additional grain, indistinguishable from the others under CL, is significantly older with a concordant age of 783 ± 7 Ma, which is broadly similar to the ages of gneisses in the Aktyuz and Kemin Complexes reported above and probably represents an inherited xenocryst.

The $\varepsilon_{Nd(t)}$ value for whole-rock sample KG 37 is −2.5, and the corresponding mean crustal residence age is 1.30 Ga (Table 5). These values favour a crustal-melt granitoid, but the Nd model age is significantly younger than in all previous samples, and we cannot exclude the possibility of mixing between old crust and a juvenile melt.

Sample KG 38 also contains perfectly euhedral magmatic zircons, and CL images commonly show wide striped and sector zoning (Fig. 16b, inset). Analysis of seven grains produced concordant and well-grouped results (Table 3) with a mean $^{206}Pb/^{238}U$ age of 472.0 ± 3.1 Ma (Fig. 16b). The $\varepsilon_{Nd(t)}$ value for whole-rock sample KG 38 is −1.9, and the corresponding mean crustal residence age is 1.35 Ga (Table 5), similar to sample KG 37. Therefore, the same interpretation as for KG 37 can be advanced, i.e. the gneiss protolith most likely is a crustal-melt granitoid, but mixing with a juvenile component cannot be excluded.

The ages and Nd isotopic characteristics of samples KG 37 and 38 are identical and reflect granodiorite emplacement in the Early Ordovician and derivation from the same or very similar sources.

Sample KG 49 is a flow-banded, undeformed and unmetamorphosed rhyolite (Fig. 17) from the presumed Neoproterozoic Burubai formation of rhyolite and ignimbrite which rests unconformably on metamorphic schists in the eastern part of Kyrgyz ridge W of Kyzyl Oktyabr village (Table 1, Fig. 2). The zircons are euhedral, short- to long-prismatic, and display excellent oscillatory, magmatic zoning under CL (Fig. 14d, inset). The analyzed six grains all gave concordant results (Table 3) and provided a mean $^{206}Pb/^{238}U$ age of 452.2 ± 2.8 Ma (Fig. 14d), which we interpret to reflect the time of lava eruption. This Late Ordovician age demonstrates that deformation and metamorphism in the Kemin Complex was over by the Mid-Ordovician, as already shown by the age of 472 Ma for the undeformed Dolpran granodiorite.

Sample KG 44 represents a plagioclase-phyric basalt of the Cholok sequence which was interpreted as part of a Cambrian island arc assemblage best developed in the Baibichen–Saur Mountains SW of Cholok village (Bakirov and Mikolaichuk, 2009) and was collected some 400 m west of Cholok Train Station near the main road from Bishkek to Kochkor (Table 1, Fig. 2). The sequence rests on felsic volcanic rocks which were previously considered to be Neoproterozoic in age, but our data show them to be Late Ordovician at 452 Ma (see sample KG 49). The zircons are mainly short-prismatic, stubby, and idiomorphic and show diffuse to well developed oscillatory

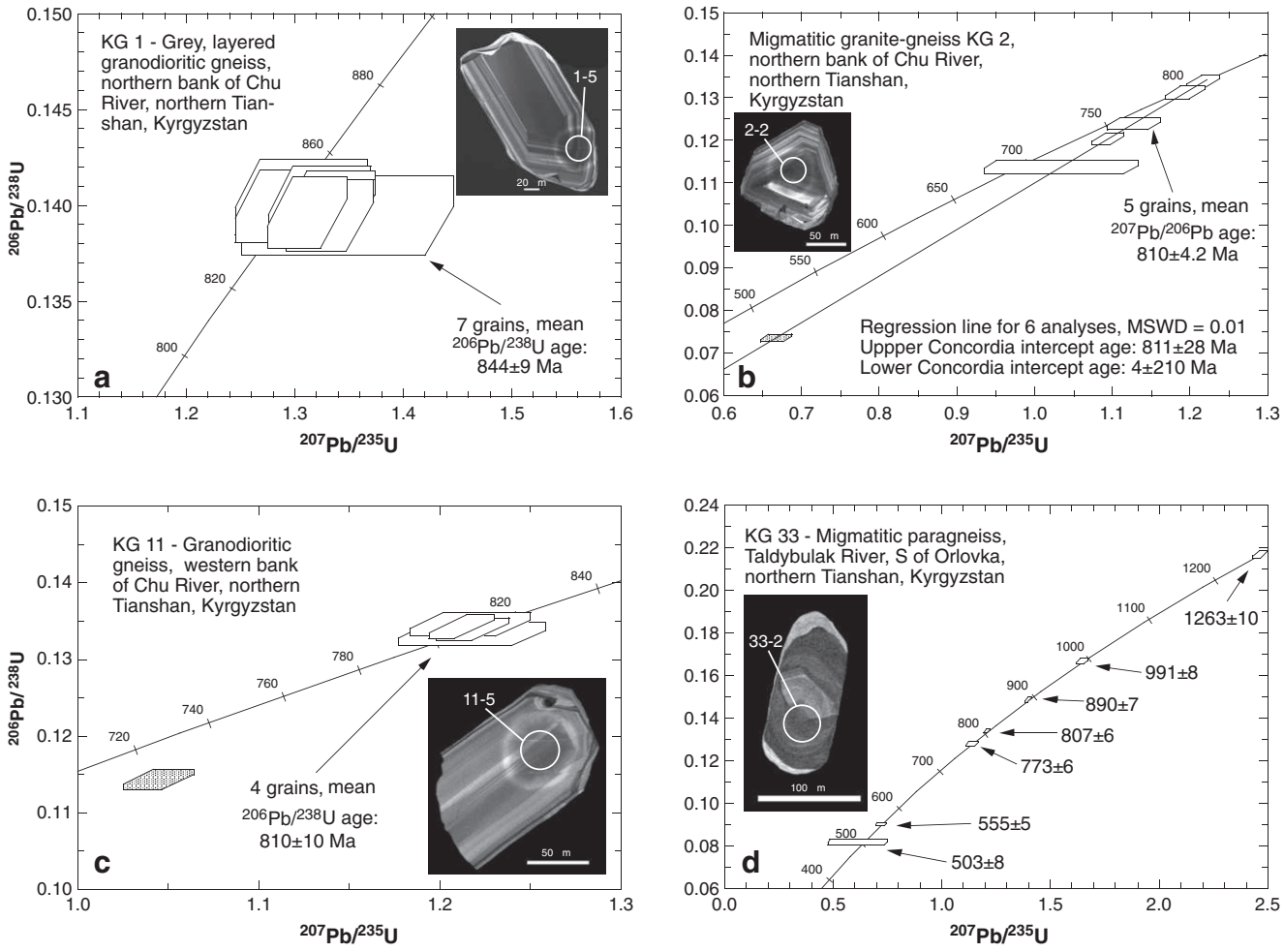

Fig. 11. Concordia diagrams showing analytical data for zircons from granitoid gneisses and a migmatitic paragneiss of the Kemin Complex. See Table 3 for details. Data boxes as in Fig. 7. Insets show cathodoluminescence images of typical zircon from each sample with number of analysis and white scale bar.

zoning (Fig. 16c, inset). Ten grains were analyzed on SHRIMP II (Table 3) of which 6 produced concordant results with a weighted mean $^{206}Pb/^{238}U$ age of 448.9 ± 5.6 Ma (Fig. 16c). Three grains are slightly to moderately discordant, but their $^{207}Pb/^{206}Pb$ ratios are identical, within error, with the concordant results suggesting recent Pb-loss, and the weighted mean $^{207}Pb/^{206}Pb$ age for all 9 analyses is 453.0 ± 5.8 Ma (Fig. 16c). Analysis KG44-9 is grossly discordant (Table 3) and was not considered in the age calculation. We interpret the age of ca. 450 Ma as reflecting the time of volcanism, and this is considerably younger than previously inferred but in line with the ages of the other post-kinematic rocks presented above.

Lastly, we dated a massive, undeformed coarse-grained leucogabbro from a small intrusion into the foliated Kopurelisai ophiolite basalts and exposed in the Kichi–Kemin River valley as shown in Fig. 2 (sample KG 42, see Table 3). The zircons are generally >100 μm in size, very euhedral and display the typical broad, striped zoning in CL images (Fig. 16d, inset) that is often found in high-temperature gabbro intrusions (Corfu et al., 2003). Twelve very homogeneous grains were dated and provided near-identical, concordant isotopic ratios (Table 3) with a weighted mean $^{206}Pb/^{238}U$ age of 320.9 ± 4.1 Ma (Fig. 16d). We interpret this to reflect the time of gabbro emplacement and, on a regional scale, this intrusion most likely belongs to the Balkash–Yili magmatic belt (Fig. 1) that characterizes a Carboniferous active margin and is developed in adjacent areas, in particular in the southern part of the Kendyktas Ridge, directly north of Aktyuz (Bekzhanov et al., 2000; Filippova et al., 2001).

5. Discussion and conclusions

Our single grain zircon ages of metamorphic and igneous rocks in the Aktyuz and Kemin Complexes of the northern Tianshan differ significantly from previously published data that were obtained through multi-grain U–Pb zircon and α-Pb dating. The main cluster of SHRIMP ages of granitoid gneisses in the Aktyuz and Kemin Complexes is around 800 Ma (778–844 Ma), which we interpret to reflect a major phase of Neoproterozoic granitoid magmatism in the Kyrgyz Northern Tianshan. Such magmatism is also documented in southern Kazakhstan, the Kyrgyz Middle Tianshan, the Chinese Tianshan and the Tarim Craton (Kiselev and Maksumova, 2001; Kröner et al., 2007; 2009; Lu et al., 2008; Long et al., 2011) but the geodynamic significance of this event is largely uncertain because of later deformation and metamorphism of the dated rocks which makes it impossible to establish the original rock relationships. In the northern Tarim craton Early Neoproterozoic granitoids include varieties with adakitic chemistry, which were interpreted to have formed by partial melting of basement rocks in a crust thickened by magmatic underplating (Long et al., 2011).

Two ages of 562 ± 7 and 540.8 ± 3.1 Ma of granitoid gneisses are significantly younger and document a later magmatic episode, possibly related to Late Neoproterozoic–Cambrian arc magmatism as suggested by the chemical characteristics of these samples. The youngest detrital zircon grain in our migmatitic paragneiss sample KG 33 from the East Kyrgyz Range yielded a SHRIMP age of 503 ± 8 Ma

Fig. 12. Field photographs of dated granitoid gneisses of the Kemin Complex. (a) Reddish-brown, layered and slightly migmatitic granite-gneiss KG 2 cut by late pegmatite dykes. (b) Grey, finely layered and ductilely deformed granodioritic gneiss KG 11 enclosing boudin of amphibolite interpreted as remnant of a mafic dyke.

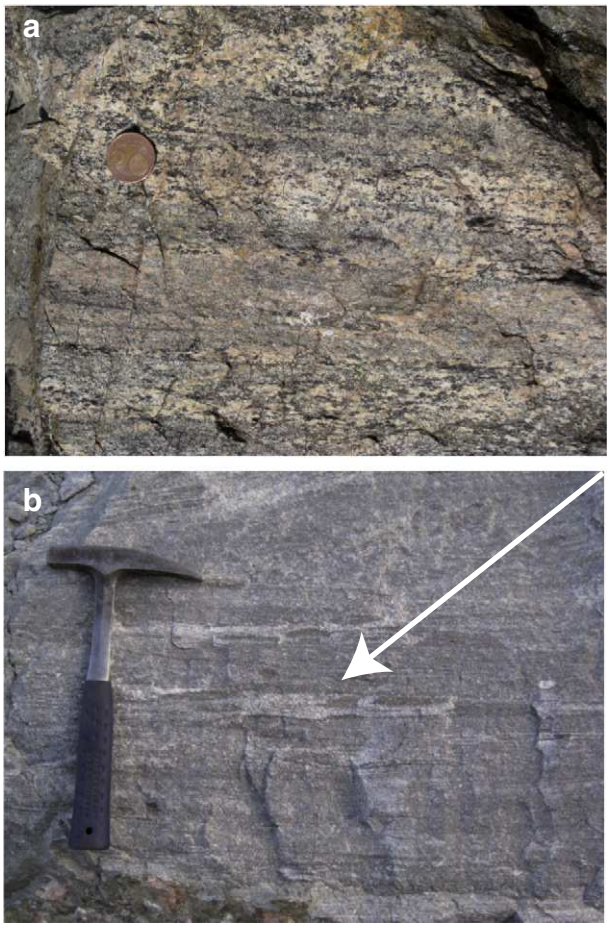

Fig. 13. Field photographs of granitic gneisses of the Kemin Complex. (a) Pink coarse-grained and well layered granite-gneiss KG 36. (b) Finely layered grey granite-gneiss with rootless isoclinal folds, see arrow.

(Table 3, Fig. 11d), which sets a maximum Late Cambrian age for deposition of the protolith sediment and constrains the age of the latest episode of migmatite formation to the Early Palaeozoic.

Our dated granitoid gneisses and migmatites in the Aktyuz and Kemin Complexes are characterized by negative $\varepsilon_{Hf(t)}$ zircon data (Table 4 and Fig. 8) and negative $\varepsilon_{Nd(t)}$ whole-rock values of ca. −5 to −12 (Table 5, Fig. 18) which imply that these rocks originated through melting of older continental crust. The Nd mean crustal residence ages of ca. ~1.5–2.1 Ga may either reflect mantle melt extraction events or, more likely, are the result of mixing of Palaeoproterozoic or older crust with variable proportions of juvenile, mantle-derived melts. The presence of widespread older crust in the northern Tianshan is evident and is also supported by a 1180 ± 9 Ma zircon xenocryst in ortho-migmatite sample KG 36 and by a 1263 ± 10 Ma detrital grain in para-migmatite sample KG 33.

We have no convincing explanation for substantial differences in the zircon Hf_c and whole-rock Nd model ages in samples KG 1 and KG 5 and suggest either decoupling of the two isotopic systems or disturbance of the Sm–Nd system during post-magmatic (metamorphic?) processes. Nevertheless, the Hf zircon data argue for chronologically very heterogeneous crustal sources for the gneiss precursors, and this supports the contention of Belousova et al. (2006), Phillips et al. (2011) and Stevens et al. (2011) that Hf isotopic signatures of granite magmas point back to the sources that have contributed to form the magmas. Interestingly, the range of zircon crust-formation ages t_{Hfc} in samples KG 1 and KG 5 from ca. 1.72 to 2.60 Ga is similar to SHRIMP zircon ages of 1.79 to 2.79 Ga for granitoid gneisses in the Anrakhai Complex exposed in the Chu–Yili Mountains of southern Kazakhstan (see Fig. 1 and Kröner et al., 2007). We therefore speculate that the northern Tianshan basement and Anrakhai may have constituted a single Precambrian block that rifted apart in the Early Cambrian due to formation of a back-arc basin in the Dzhalair–Naiman area (see discussion below and Fig. 19a and b).

High-pressure eclogites, mostly retrograded to garnet amphibolite, form distinct layers and boudins in the granitoid gneisses of Aktyuz and originated from gabbroic dykes which were rotated into parallelism with the enclosing gneisses and disrupted during high-grade ductile deformation. This is a common feature in high-grade terranes and has been described from numerous localities worldwide (see Myers, 1978, and Passchier et al., 1990, for review and examples). Field relations demonstrate that gneisses and mafic dykes represent a coherent tectonic assemblage and jointly underwent HP metamorphism which led to formation of eclogites in mafic rocks. Because of extensive retrogression and unsuitable chemical composition the felsic granitoid gneisses do not preserve the HP mineralogy.

The gneiss-eclogitic gabbro dyke relationship in the Aktyuz Complex is identical to that in many high-grade gneisses worldwide. For instance, in the Hengshan Complex of the North China Craton 1.92 Ga gabbroic dykes intruded into Late Archaean to Early Palaeoproterozoic tonalitic to granodioritic gneisses and were strongly deformed and metamorphosed to eclogite-facies at 1.85 Ga before becoming retrogressed and partly mylonitized (Kröner et al., 2005, 2006; O'Brien et al., 2005). Similar relationships were described from the Archaean Aldan Shield in Siberia (Smelov and Beryozkin,

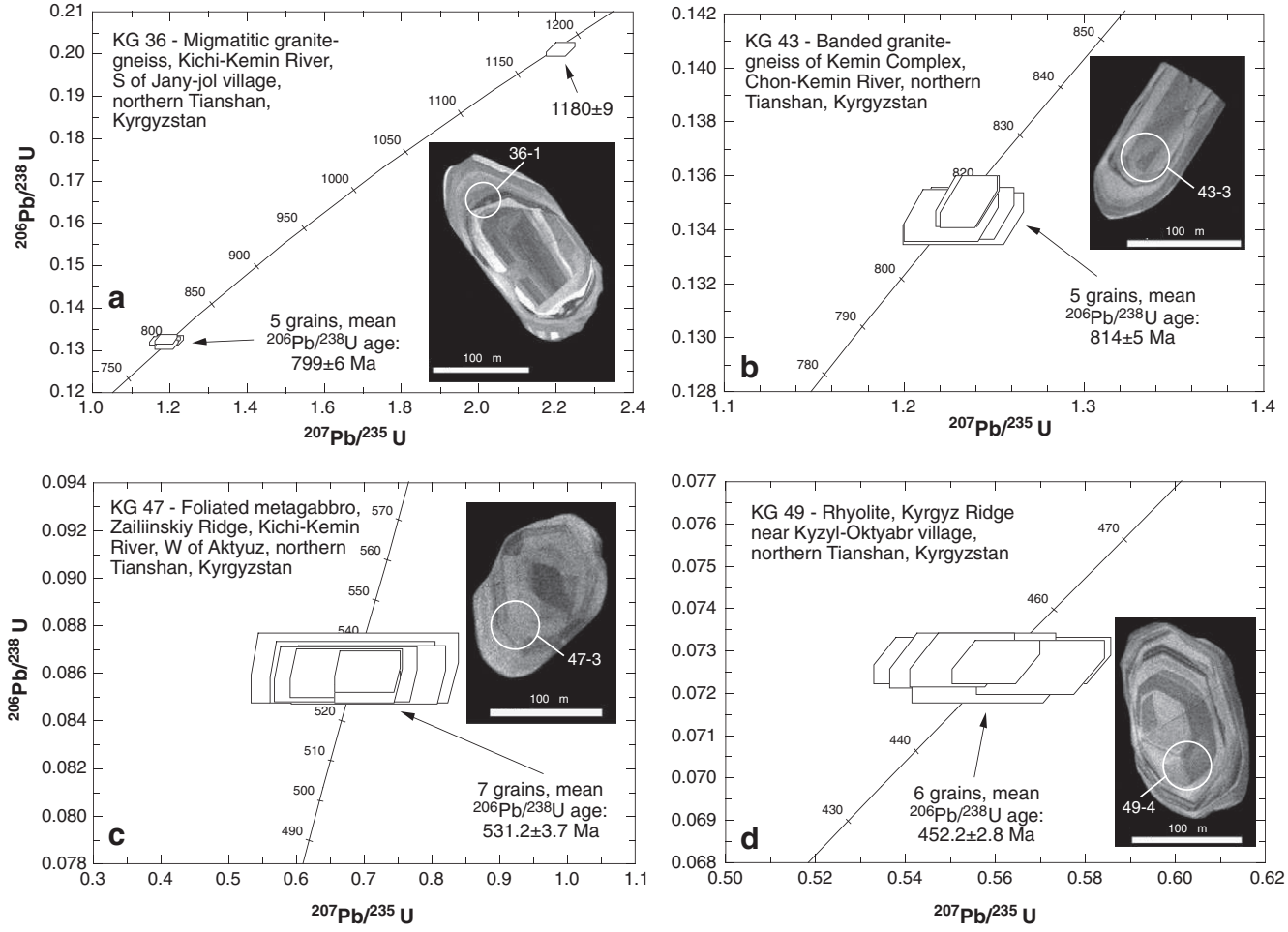

Fig. 14. Concordia diagrams for zircon analyses from granite-gneisses of the Kemin Complex (a and b), a gabbro of the Kopurelisai suite (c), and a rhyolite of the Burubay formation (d). Errors as in Fig. 7. Insets show cathodoluminescence images of typical zircon from each sample with number of analysis and white scale bar.

1993), the Palaeoproterozoic Belomorian belt in Karelia (Kozlovsky and Aranovich, 2008; Koslovskii and Aranovich, 2010), the Glenelg-Attadale Inlier of the NW Highlands of Scotland (Storey, 2008), and the Caledonides of East Greenland (Elvevold and Gilotti, 2000). Although Orozbaev et al. (2010) maintained that the Aktyuz granitoid gneisses did not experience the same HP metamorphic evolution as the interlayered mafic dykes, we are confident that the entire package must have been transferred to eclogite depths, and we suggest that rehydration during amphibolite- to greenschist-facies retrogression has completely eradicated the evidence for the HP-event in the quartzo-feldspathic rocks.

This interpretation is also suggestive for the Aktyuz occurrence and is supported by a clockwise P–T path for the eclogites (Orozbaev, et al. 2007). Possible subduction of continental crust in the region was also considered for an adjacent area to the north in southern Kazakhstan by Avdeev and Kovalev (1989) who found that middle Ordovician conglomerates contain pebbles of Neoproterozoic (?) rhyolites which are metamorphosed to lawsonite–glaucophane schist.

The Aktyuz mafic dykes are younger than ~780 Ma, based on the age of granitic gneisses into which they intruded. The age of the metamorphic event responsible for the high-grade foliation in both gneisses and mafic rocks is <540 Ma, based on the youngest age of our dated K-feldspar-rich granitoid gneiss. This is confirmed by our $^{39}Ar/^{40}Ar$ muscovite ages of 470–475 Ma for two Aktyuz granite-gneiss samples. The eclogite metamorphism in the Aktyuz Complex is also likely to have been part in this Early Paleozoic metamorphic event. We do not consider the whole-rock/mineral Rb–Sr isochron "age" of 749 ± 14 Ma reported by Tagiri et al. (1995) for an Aktyuz eclogite sample to accurately reflect the age of metamorphism because garnet in the analyzed sample is not in equilibrium with the other minerals and with the whole-rock, and amphibole represents a product of retrogression (Bakirov et al. 2003).

Ophiolitic complexes in southern Kazakhstan and the northern Tianshan of Kyrgyzstan were dated by palaeontological and isotopic methods as Cambrian (Kröner et al., 2007; Ryazantsev et al., 2009) and Cambrian to earliest Ordovician (Mikolaichuk et al., 1997; Ghes' 2008). The metamorphosed Kopurelisai ophiolite suite, traditionally interpreted as Proterozoic, represents the only exception, and the age of this suite is critical for reconstructing the overall history of the region. Our zircon age of 531.2 ± 3.7 Ma for leucogabbro sample KG 47 confirms an Early Cambrian age for the Kopurelisai ophiolite suite and implies a possible genetic link with the Dzhalair–Naiman ophiolite belt of southern Kazakhstan where similar ages of 513 ± 4; 519 ± 4; and 521 ± 2 Ma were reported for ophiolitic plagiogranites (Kröner et al., 2007; Ryazantsev et al., 2009). Our new data effectively rule out a Palaeoproterozoic age for the ophiolite and suggest formation of an Early Cambrian ocean basin in southern Kazakhstan and northern Kyrgyzstan.

The age of ca. 472 Ma for the Dolpran post-tectonic granodiorite reflects an episode of Early Ordovician granitoid magmatism which is documented at several locations in the northern Tianshan (Kiselev, 1999; Ghes', 2008). The presence of an inherited 783 ± 7 Ma zircon in one of the dated samples may be the reason for an older, discordant apparent zircon age of 692 ± 15 Ma that was previously reported for

Fig. 15. (a) Deformed Dolpran quartz–diorite (KG 37) with elongate gabbro xenolith. (b) Undeformed Dolpran quartz–diorite sample KG 38.

the same pluton by conventional multigrain dating (Kiselev et al., 1993). These Early Ordovician granitoids with arc signatures may either be related to collision of the North Tianshan and Anrakhai microcontinents (Bakirov and Maksumova, 2001; Ghes' 2008) or reflect an early phase of magmatic arc formation in the northern Kyrgyz Tianshan during the late Early and Middle Ordovician (Lomize et al., 1997).

Neoproterozoic and Cambrian protolith ages for high-grade granitoid gneisses in the Aktyuz block rule out an assumed Neoproterozoic age for the unmetamorposed rhyolites of the Burubai formation which rest unconformably on metamorphic rocks. Our Late Ordovician zircon age of 451.9 ± 4.6 Ma for a rhyolite in the eastern part of the Kyrgyz Ridge (Fig. 2) corresponds to the main episode of collisional granitoid magmatism in the northern Tianshan (Kiselev and Maksumova, 2001; Djenchuraeva et al., 2008; Ghes', 2008; Glorie, et al., 2010). Despite the extensive occurrence of Late Ordovician and Silurian granites, co-magmatic volcanic equivalents are essentially unknown in this region, and the above result is first direct evidence for syn-collisional Late Ordovician volcanic activity in the northern Tianshan.

The zircon ages for metamorphic assemblages, ophiolitic gabbro and post-kinematic igneous rocks indicate that the Aktyuz terrane is not a part of a coherent Precambrian continental domain but constitutes a package of tectonic slivers, made up of Proterozoic continental and Early Palaeozoic ophiolitic rocks, which underwent medium- to high-grade metamorphism in the Early Palaeozoic. The time of this metamorphism is constrained between 503 ± 8 and 472 ± 3 Ma, based on the youngest detrital zircon age in the metamorphic rocks and the age of the post-kinematic Dolpran pluton. This reflects a latest Cambrian to earliest Ordovician orogenic event which is also documented by structural unconformities in many areas of southern Kazakhstan and the northern Tianshan (Abdulin, 1986; Bakirov and Maksumova, 2001; Kiselev and Maksumova, 2001; Ghes', 2008).

Palaeotectonic reconstructions of southern Kazakhstan and the northern Tianshan suggest that the evolution of the Early Palaeozoic fold belt was generally controlled by convergence and collision of the North Tianshan and Anrakhai microcontinents after closure of the Dzhalair–Naiman ophiolite basin (Fig. 1) (Avdeev and Kovalev, 1989; Bakirov and Maksumova, 2001; Kiselev and Maksumova, 2001; Ghes', 2008; Alexeiev et al., in press).

Similar ages of Neoproterozoic felsic magmatic rocks which are developed on both sides of the Dzhalair–Naiman belt in the Aktyuz area (840–780 Ma, this study) and in the South Chu–Yili Mountains of Kazakhstan (776–741 Ma, Kröner et al., 2007) as well as similarities in Palaeoproterozoic to Archaean basement ages imply that the North Tianshan and Antrakhai blocks were part of the same continent in the Neoproterozoic (Fig. 19a). Comparable ages for the youngest granitoid gneisses at Aktyuz (562–541 Ma, this study) and a metadacite in the Anrakhai area (534 Ma, Kröner et al., 2007) also suggest a single continental margin arc which evolved in the Latest Precambrian and Early Cambrian prior to opening of the Dzhalair–Naiman basin (Fig. 23b) and was presumably connected with subduction from the northeast (Fig. 19a). The Dzhalair–Naiman basin (Fig. 19b) opened in the Early to Middle Cambrian some 531–513 Ma ago (Kröner et al., 2007; Ryazantsev et al., 2009, this study) and most likely represents a back-arc basin with respect to the Anrakhai arc (Fig. 19b) (Alexeiev et al., in press).

Convergence of the Anrakhai and Aktyuz microcontinents was connected with subduction of oceanic lithosphere of the Dzhalair–Naiman basin towards the northeast during the Late Cambrian and Early Ordovician. The direction of subduction is implied by obduction of ophiolite slivers of the Dzhalair–Naiman belt onto the Precambrian North Tianshan microcontinent (Bakirov and Maksumova, 2001; Ghes', 2008) as well as by a weakly expressed southern structural vergence of the collisional belt and by the location of a Late Cambrian arc (509 Ma) in the NE of the accretionary complex (Alexeiev et al., in press). A top-to the-south sense of motion is also inferred in the Aktyuz Complex from the orientation of overturned folds in the gneisses (Bakirov, 1978) and is consistent with the reconstructed polarity of the above subduction system (Fig. 19c and d).

The timing of subduction is based on the Late Cambrian and Early Ordovician age of turbidites which were deposited in the Dzhalair–Naiman basin. Subduction was accompanied by exhumation of HP garnet pyroxenites in the internal part of the accretionary complex along the boundary with the arc in the NE of the Anrakhai area (Fig. 19c and d) (see Alexeiev et al., in press for details). Passive margin shelf sedimentation in the northern Tianshan continued from the Late Cambian to the Early Ordovician and terminated in Floian time (Keller and Rukavishnikova, 1961) when apparently collision began (Fig. 19d).

Granitoid gneisses and HP rocks of the Aktyuz Complex were most likely formed in the lower plate, and we suggest that the gneisses represent a fragment of the North Tianshan microcontinent which was involved in subduction and reached the depth of HP eclogite-facies. Deep subduction of the edge of the continent may have been caused by slab pull from the descending oceanic lithosphere (Fig. 19e). The Aktyuz gneisses and HP rocks were thrust onto the greenschist-facies Kopurelisai meta-ophiolites (Bakirov et al., 2003) of which a gabbro was dated as Early Cambrian (this study). Field relationships between the high- and low-pressure rocks suggest that a fragment of the subducted edge of the North Tianshan microcontinent (i.e. the Aktyuz Complex) was detached from the descending slab, exhumed due to high buoyancy, and finally wedged into thrust sheet packages consisting of Neoproterozoic granite-gneiss and Early Palaeozoic meta-ophiolite fragments and metasediments (Fig.19e).

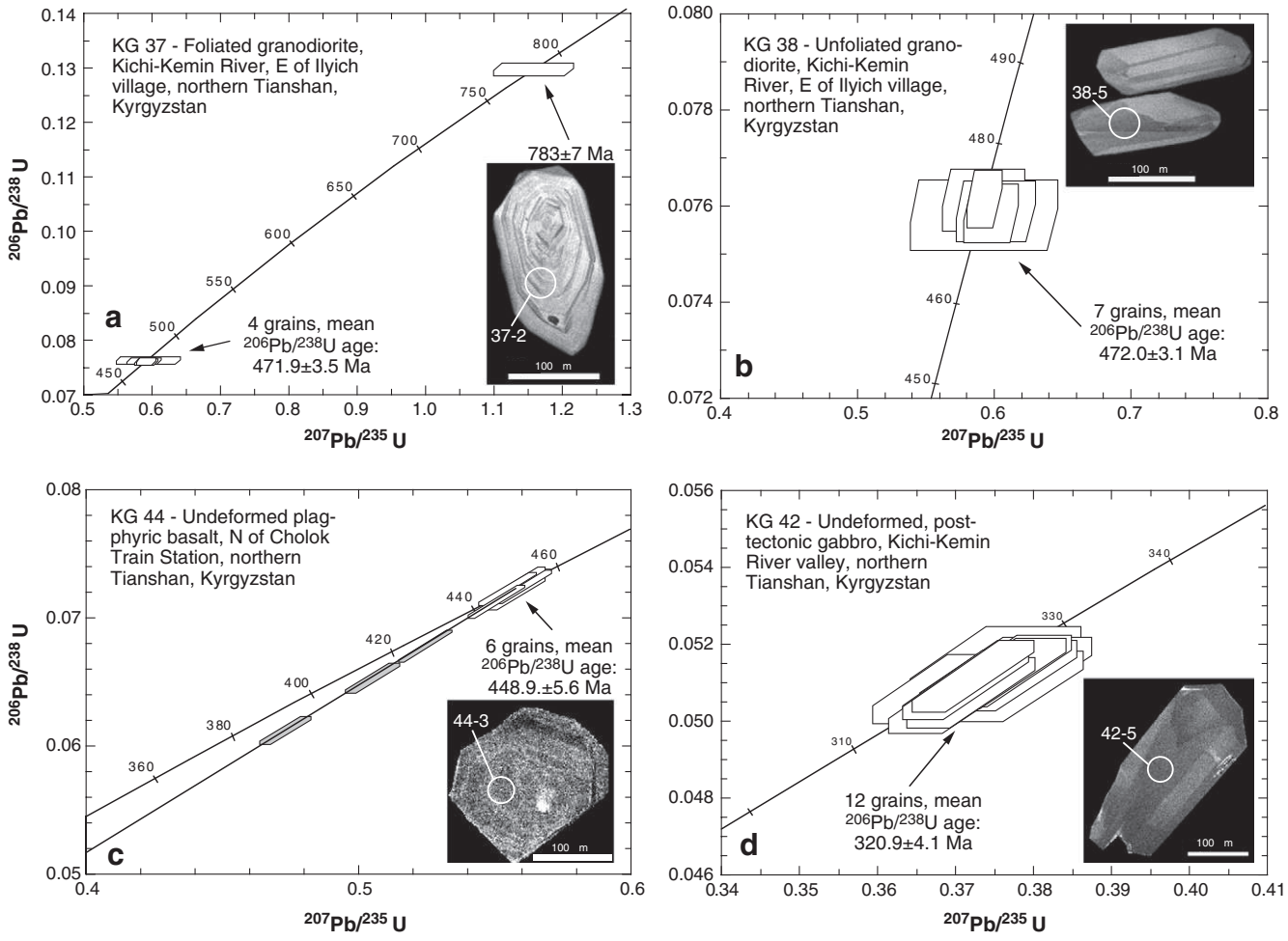

Fig. 16. Concordia diagrams showing zircon analyses from the Dolpran Pluton (a and b) and postkinematic magmatic rocks (c and d). (a) Foliated granodiorite sample KG 37. (b) Unfoliated hornblende–granodiorite sample KG 38. (c) Undeformed plagioclase-phyric basalt of Cholok Sequence. (d) Undeformed gabbro intruding Kopurelisai ophiolite. Data boxes as in Fig. 7. Insets show cathodoluminescence images of typical zircon from each sample with number of analysis and white scale bar.

General uplift and erosion of the entire metamorphic block including the Aktyuz, Kemin and Kopurelisai Complexes occurred soon after the main metamorphic event, based on a middle Ordovician Darriwilian (Llanvirnian) age of overlap sedimentary assemblages (Bakirov and Mikolaichuk 2009). This may reflect uplift of the subducted microcontinental margin after break-off of the oceanic slab (Fig. 19f).

Our present study shows that the Late Cambrian–Early Ordovician orogeny affected a significantly broader belt than previously thought,

Fig. 17. Undeformed, flow-banded rhyolite sample KG 49.

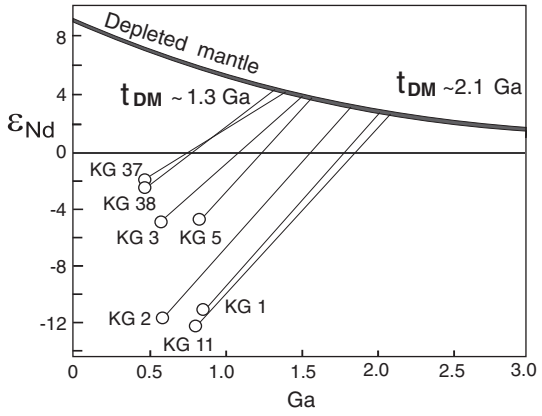

Fig. 18. Nd isotope evolution diagram for whole-rock samples of selected granitoid rocks of the Aktyuz Complex (KG 3 and 5) Kemin Complex (KG 1, 2, and 11) and postkinematic Dolpran pluton (KG 37 and 38). Depleted mantle curve after DePaolo (1988).

and large fragments of continental crust, most likely derived from the microcontinent of the northern Tianshan, were involved in subduction, became tectonically interlayered with ophiolite slivers, and underwent medium- and high-grade metamorphism. Similar patterns with structural interlayering of tectonic slivers with Palaeozoic ophiolites, Precambrian felsic igneous rocks and passive margin sediments characterize a major part of the Kyrgyz northern Tianshan, including the Makbal block in the West Kyrgyz Ridge as well as the Dzhalair–Naiman and Anrakhai belts in the Chu–Yili Mountains of southern Kazakhstan. Stratigraphic and structural data as well as isotopic dating constrain the major deformation event in these areas to the Early Ordovician (Abdulin 1980; Avdeev and Kovalev, 1989;

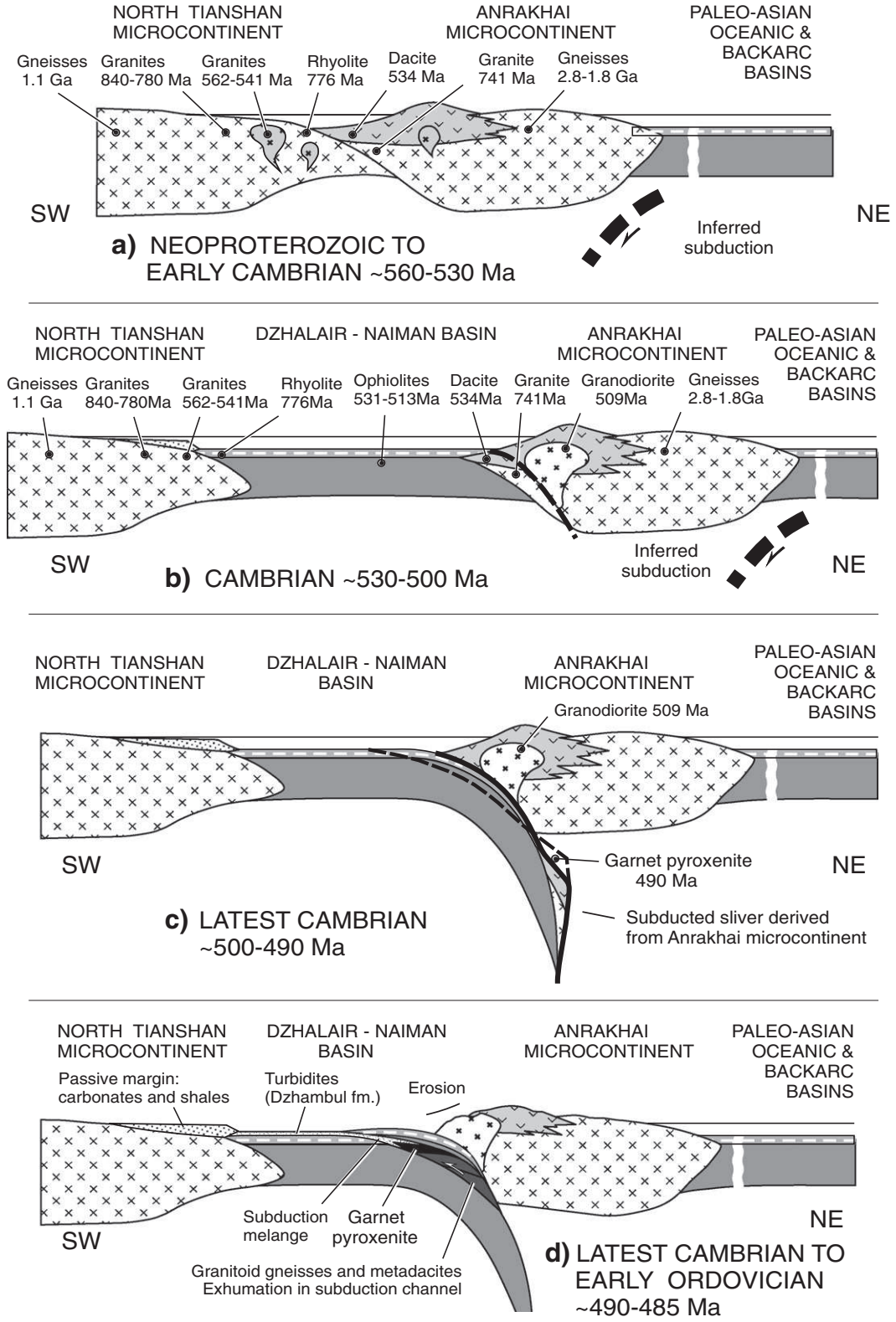

Fig. 19. Cartoons showing suggested tectonic setting and evolution of the Kyrgyz northern Tianshan during the Neoproterozoic to Early Palaeozoic. For explanation see text.

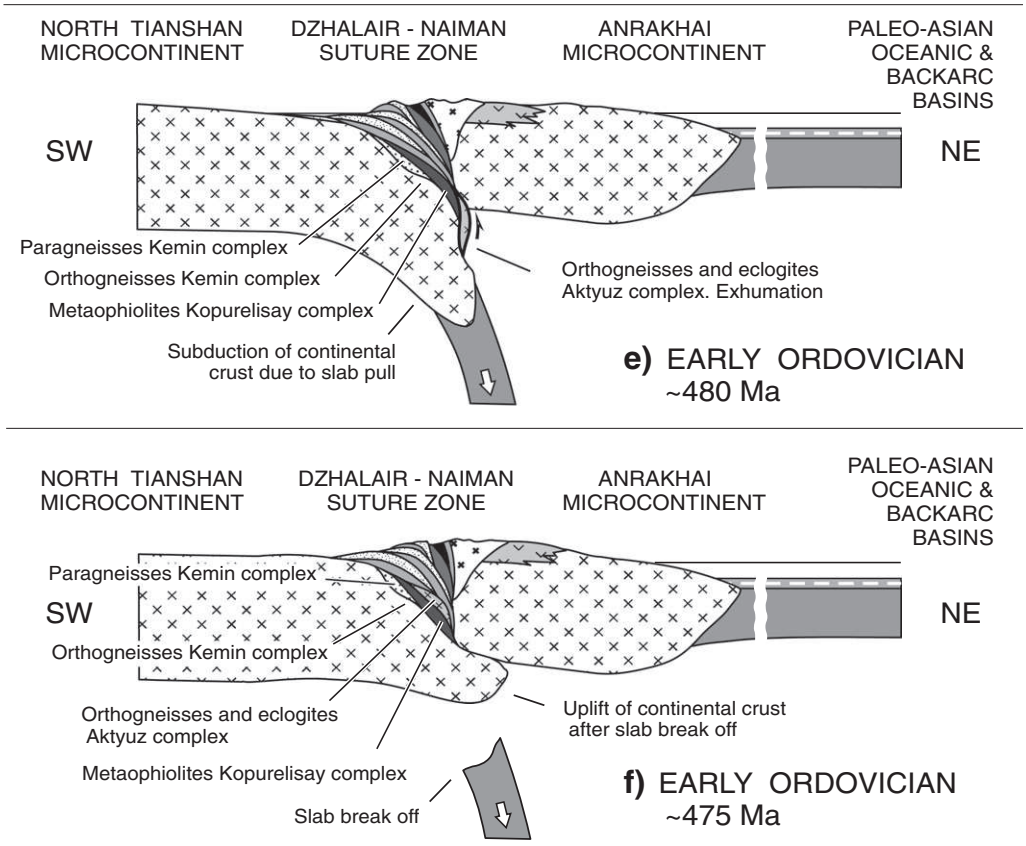

Fig. 19 (*continued*).

Lomize et al., 1997; Mikolaichuk et al., 1997; Bakirov and Maksumova 2001; Ghes' 2008; Alexeiev et al., in press).

Similar structural patterns and similar ages for the major deformation episode at ~480 Ma within the entire KNT belt suggest the existence of a distinct major tectonic unit, i.e. an agglomeration of continental, ophiolitic and HP metamorphic belts, which were welded together prior to the Middle Ordovician and acted as a centre of nucleation within the evolving CAOB for further tectonic accretion in Kazakhstan and the Tianshan during the Palaeozoic.

Acknowledgements

We thank A.B. Bakirov, K.S. Sakiev, V.V. Kiselev, F. Apayarov and A.V. Mikolaichuk for discussion, help with selecting targets and important comments that improved the manuscript. H. Zhou of the Beijing SHRIMP Centre provided the zircon CL images, and Q. Ye and H. Tao prepared perfect zircon mounts. Jianfeng Gao of Hong Kong University kindly provided an unpublished Excel-based program to construct the Hf evolution diagrams of Fig. 8. We also thank Bo Wang and Reimar Seltmann for constructive reviews. This study was supported by Deutsche Forschungsgemeinschaft (DFG) grant KR590/90-1 to AK, the Russian Foundation for Basic Research grant 09-05-91331-NNIO-a and Program N10 of the Earth Science Department of RAS to DVA and AAT, and by the Beijing SHRIMP Centre, China. It is also part of a collaborative study between Mainz University and The University of Hong Kong, funded jointly by the German Exchange Service (DAAD) and the Hong Kong Research Council, and is a contribution to the Mainz Earth System Research Centre.

Appendix A. Analytical procedures

Whole-rock samples some 3–6 kg in weight were crushed to <60 mesh at Mainz University by standard procedures using a jaw crusher and steel rolling mill. Some 100 g of the homogenized crush was then pulverized for chemical analysis in a ring mill using a hardened tungsten carbide steel vessel. The remaining material was fed over a Wilfley table to obtain a heavy mineral concentrate including zircons.

Major and trace element chemistry

Major element compositions of the dated whole-rock samples were determined with a Rigaku ZSX100e X-ray fluorescence spectrometer on fused glass disks at the Guangzhou Institute of Geochemistry, Chinese Academy of Sciences, with analytical uncertainties between 1 and 5%. Trace elements were analyzed using a Perkin-Elmer Sciex ELAN 6000 ICP-MS, following procedures described by Li (1997). About 50 mg of powdered sample was digested with mixed $HNO_3 + HF$ acid in steel-bomb coated Teflon beakers in order to assure complete dissolution of the refractory minerals. Rh was used as an internal standard to monitor signal drift, and the USGS rock standards GSP-1, G-2, W-2 and AGV-1 and the Chinese national rock standards GSR-1 and GSR-3 were analyzed in order to calibrate element concentrations of the unknown samples. Analytical uncertainties for the trace elements were generally better than 5%.

SHRIMP zircon dating and cathodoluminescence imaging

Heavy mineral concentrates obtained from the Wilfley-table were further purified by conventional magnetic and heavy mineral separation methods. Zircons were handpicked and mounted in epoxy resin together with chips of the Perth Consortium zircon standard CZ3 in the Beijing SHRIMP Centre, Chinese Academy of Geological Sciences. The mount was ground down and polished so that the zircon interiors were exposed, and zircons were photographed in reflected and transmitted light and under cathodoluminescence (CL)

to enable easy and best location on the mount during SHRIMP analyses. The mount was then cleaned and gold-coated. CL imaging of the sectioned zircons was performed in the Beijing SHRIMP Center using a Hitachi S-3000 N scanning electron microscope (accelerating voltage 10 kV, beam current 109 mA).

Isotopic analyses were performed on the SHRIMP II sensitive high-resolution ion-microprobe of the Beijing SHRIMP Centre whose instrumental characteristics were described by De Laeter and Kennedy (1998). The analytical procedures were outlined in Compston et al. (1992), Claoué-Long et al. (1995), Nelson (1997) and Williams (1998). Prior to each analysis, the surface of the analysis site was precleaned by rastering of the primary beam for 2–3 min, to reduce or eliminate surface common Pb. The reduced $^{206}Pb/^{238}U$ ratios were normalized to 0.09432, which is equivalent to the adopted age of 564 Ma for CZ3. Pb/U ratios in the unknown samples were corrected using the ln(Pb/U)/ln(UO/U) relationship as measured in standard CZ3 and as outlined in Compston et al. (1984) and Nelson (1997).

For data collection, six scans through the critical mass range were made. Primary beam intensity was between 4 and 6 nA, and a Köhler aperture of 100 μm diameter was used, giving a slightly elliptical spot size of about 30 μm. Peak resolution at 1% peak height was about 5000, enabling clear separation of the ^{208}Pb-peak from the HfO peak. Sensitivity was about 20 cps/ppm/nA Pb on the standard CZ3. Analyses of samples and standards were alternated to allow assessment of Pb^+/U^+ discrimination. The 1-sigma error of the $^{206}Pb/^{238}U$ ratio during analysis of all standard zircons during this study was between 0.7 and 1.2%. Raw data reduction and error assessment followed the method described by Nelson (1997). Common-Pb corrections were applied using the ^{204}Pb-correction method. Because of very low counts on ^{204}Pb in most samples it was assumed that common lead is surface-related (Kinny, 1986), and therefore the isotopic composition of Broken Hill lead was used for correction. The analytical data are presented in Table 3. Errors of individual analyses are given at the 1-sigma level and are based on counting statistics and include the uncertainty in the U/Pb age of the standard, added in quadrature (Nelson, 1997). Errors of pooled analyses are reported at the 2 sigma confidence interval. The data are graphically presented on conventional concordia diagrams.

Sm–Nd isotopic analysis

Whole-rock sample powders and mineral concentrates were dissolved in Teflon bombs in a mixture of 2 ml concentrated HF and ~100 μl $HClO_4$ over 5 days at ca. 180 °C. The LREE were separated on a quartz column with a 5 ml resin bed of AG 50 W-X12 of 200–400 mesh. Sm and Nd were then separated from the LREE fraction on a quartz column filled with 1.7 ml Teflon powder coated with di-ethylhexylphosphoric acid (HDEHP). Sm and Nd were loaded with diluted phosphoric acid on a Re-filament and measured as metal in double filament configurations. Total procedural blanks of <200 pg for Nd and Sm are not significant for the processed amounts of Sm and Nd. Isotope compositions were analyzed on an upgraded MAT 261 mass spectrometer, and Nd isotope abundance ratios were determined with a dynamic triple-collector routine. Nd and Sm concentrations were determined in a static data collection routine, and $^{143}Nd/^{144}Nd$ ratios were normalized to $^{146}Nd/^{144}Nd = 0.7219$, using an exponential fractionation law. During this study the La Jolla Nd reference material yielded $^{143}Nd/^{144}Nd = 0.511847 \pm 0.000008$ (2 SD of population, N = 10). The long-term external precision for $^{143}Nd/^{144}Nd$ is estimated at 1.1×10^{-5} (2 SD). Errors of the mean $^{143}Nd/^{144}Nd$ ratios are given at the 95% confidence interval, and the analytical data are presented in Table 5.

Lu–Hf isotopic analysis

Zircon spots on zircons from two samples, most of which were previously analyzed on SHRIMP II, were selected for Hf isotopic analyses on a Nu Plasma HR MC-ICP-MS (Nu Instruments, UK), coupled to a 193 nm excimer laser ablation system (RESOlution M-50, Resonetics LLC, USA), installed in the Dept. of Earth Sciences, University of Hong Kong. The instrumental settings are detailed in Xia et al. (in press). Data were acquired by ablating 55 μm (diameter) laser spots, and a 10 Hz repetition rate was used. The analyses consisted of a 30 s blank measurement prior to the start of ablation and 40 s of ablation. The measured isotopic ratios of $^{176}Hf/^{177}Hf$ were normalized to $^{179}Hf/^{177}Hf = 0.7325$, using an exponential correction for mass bias. Isobaric interference of ^{176}Yb and ^{176}Lu on ^{176}Hf was corrected by monitoring ^{172}Yb and ^{175}Lu respectively. The in-situ measured $^{173}Yb/^{172}Yb$ ratio was used for mass bias correction for both Yb and Lu because of their similar physicochemical properties. Ratios used for the corrections were 0.5887 for $^{176}Yb/^{172}Yb$ and 0.02655 for $^{176}Lu/^{175}Lu$ (Vervoort et al., 2004). External corrections were applied to all unknowns, and standard zircons 91500 and GJ were used as external standards and were analyzed twice before and after every 10 analyses. The measured $^{176}Lu/^{177}Hf$ ratios and a ^{176}Lu decay constant of 1.865×10^{-11} a^{-1} as reported by Scherer et al. (2001) were used to calculate initial $^{176}Hf/^{177}Hf$ ratios. Calculation of ε_{Hf} values is based on the chondritic values of $^{176}Hf/^{177}Hf$ and $^{176}Lu/^{177}Hf$ as reported by Blichert-Toft and Albarède (1997). The mantle extraction model age (t_{HfDM}) was calculated using the measured $^{176}Lu/^{177}Hf$ of the zircon, but this only provides a minimum age for the source material of the magma from which the zircon crystallized. Therefore, we also calculated 'crustal' model ages t_{Hfc}, (Table 4), which assume that the parental magma of the zircons was produced from an average continental crust but was ultimately derived from the depleted mantle. $^{176}Lu/^{177}Hf$ ratios for the average crust reported in the literature vary between 0.008 (Taylor and McLennan, 1985) and 0.015 (Griffin et al., 2000; Belousova et al., 2006). Use of the higher ratio for our data results in t_{Hfc} ages which are much higher than corresponding whole-rock Nd model ages (see Table 5), and we therefore consider a ratio of 0.01 to more realistically reflect the $^{176}Lu/^{177}Hf$ ratio of our samples. The depleted mantle lines in Fig. 12 are defined by present-day $^{176}Hf/^{177}Hf = 0.28325$ and $^{176}Lu/^{177}Hf = 0.0384$ (Griffin et al., 2004), and the analytical data are presented in Table 4.

$^{40}Ar/^{39}Ar$ age determinations

Muscovite separates were obtained after crushing and handpicking of single grains ranging from 0.5 to 1 mm under a binocular microscope. The minerals were repeatedly cleaned ultrasonically in distilled water and were co-irradiated for 30 h in the nuclear reactor at McMaster University, Hamilton, Canada, in position 5c, along with a Hb3gr hornblende monitor (1072 Ma; Turner et al., 1971)). $^{40}Ar/^{39}Ar$ analyses were performed at the Geoazur Laboratory in Nice. Two muscovite grains were heated with a CO_2 Synrad laser. The gas was purified in a stainless and glass extraction line using two Al–Zr getters (working at 400 °C and ambient temperature, respectively) and a liquid nitrogen cold trap. Isotopic measurements were performed with a VG3600 mass spectrometer and a Daly-photomultiplier system. Blank measurements were obtained before and after every three sample runs (Table 5). The correction factors for interfering isotopes correspond to $(^{39}Ar/^{37}Ar)_{Ca} = (7.30 \pm 0.28) \times 10^{-4}$; $(^{36}Ar/^{37}Ar)_{Ca} = (2.82 \pm 0.03) \times 10^{-4}$ and $(^{40}Ar/^{39}Ar)_K = (2.97 \pm 0.06) \times 10^{-2}$. Ages were calculated using the ArArCalc program (Koppers, 2002), the decay constants recommended by Steiger and Jäger (1977), and an air $^{40}Ar/^{36}Ar$ ratio of 298.56 ± 0.1% (at 1 σ) (Lee et al., 2006). *J*-values ranged from 0.0035309 ± 0.0000177 (=0.5% at 1 σ) to 0.0035312 ± 0.0000177 (=0.5% at 1 σ). Mass discrimination values range from 1.00474 to 1.00738 ± 1% (1 σ) per Dalton (atomic mass unit). The criteria for defining plateau ages were as follows: 1) a plateau age should contain at least 70% of the released ^{39}Ar; 2) there should be at least three successive steps in the plateau; and 3) the integrated age of the plateau should agree with each apparent age of the plateau within a 1σ error confidence interval. Detailed $^{40}Ar/^{39}Ar$ results are shown in Table 5 and age spectra in Fig. 11.

References

Abdulin, A.A. (Ed.), 1980. Chu-Yili Ore Belt, Part 1: Geology of the Chu-Yili region. Nauka, Alma-Ata, p. 504 (in Russian).

Alexeiev, D.V., Ryazantsev, A.V., Kröner, A., Tretyakov, A.A., Xia, X., Liu, D.Y., in press. Early Ordovician high-pressure belt in the Chu-Yili Mountains: implications for the earliest stages of accretion in Kazakhstan and the Tianshan. Journal of Asian Earth Sciences, doi:10.1016/j.jseaes.2010.09.004.

Avdeev, A.V., Kovalev, A.A., 1989. Ophiolites and Evolution of the Southwestern Part of the Ural–Mongolia Folded Belt. Moscow University Publishing, Moscow, USSR, 227 pp. (in Russian).

Bakirov, A.B., 1978. Tectonic Position of Metamorphic Complexes of Tien Shan. Ilim Publishing House, Frunze, p. 262 (in Russian).

Bakirov, A.B., Korolev, V.G., 1979. The age of oldest rocks in Tianshan. Izvestiya AN SSSR. Geological Series 7, 15–25 (in Russian).

Bakirov, A.B., Maksumova, R.A., 2001. Geodynamic evolution of Tien Shan lithosphere. Geologia and Geophysica 42, 1435–1443 (in Russian).

Bakirov, A.B., Mikolaichuk, A.V. (Eds.), 2009. Tectonic evolution and crustal structure of the Tien-Shan and related terranes in the Central Asian Orogenic belt. Excursion guidebook. Bishkek, CAIAG. 123 p.

Bakirov, A.B., Tagiri, M., Sakiev, K.S., Ivleva, E.A., 2003. The Lower Precambrian rocks in the Tien Shan and their geodynamic setting. Geotectonics 37, 368–380.

Bekzhanov, G.R., Koshkin,, V.Ya., Nikitchenko, I.I., Skrinnik, L.I., Azizov, T.M., Timush, A.V., 2000. Geological Structure of Kazakhstan. Academy of Mineral Resources of the Republic of Kazakhstan, Almaty, p. 196 (in Russian).

Belousova, E.A., Griffin, W.L., O'Reilly, S.Y., 2006. Zircon crystal morphology, trace element signatures and Hf isotope composition as a tool for petrogenetic modelling: examples from eastern Australian granitoids. Journal of Petrology 47, 329–353.

Black, L.P., Jagodzinski, E.A., 2003. Importance of establishing sources of uncertainty for the derivation of reliable SHRIMP ages. Australian Journal of Earth Sciences 50, 503–512.

Black, L.P., Kamo, S.L., Allen, C.M., Aleinikoff, J.N., Davis, D.W., Korsch, R.J., Foudoulis, C., 2003. TEMORA-1: a new zircon standard for Phanerozoic U–Pb geochronology. Chemical Geology 200, 155–170.

Blichert-Toft, J., Albarède, F., 1997. The Lu–Hf geochemistry of chondrites and the evolution of the mantle–crust system. Earth and Planetary Science Letters 148, 243–258.

Botcharnikov, R.E., Almeev, R.R., Koepke, J., Holtz, F., 2008. Phase relations and liquid lines of descent in hydrous ferrobasalt—implications for the Skaergaard intrusion and Columbia River flood basalts. Journal of Petrology 49, 1687–1727.

Bowen, R., 1988. Isotopes in the Earth Sciences. Elsevier, Amsterdam, p. 490.

Chakabaev, S.E. (Ed.), 1979. Geological Map of Kazakh SSR, scale 1:500,000, South Kazakhstan Series. Aerogeologiya, Leningrad (in Russian).

Claoué-Long, J.C., Compston, W., Roberts, J., Fanning, C.M., 1995. Two Carboniferous ages: a comparison of SHRIMP zircon dating with conventional zircon ages and $^{40}Ar/^{39}Ar$ analyses. Society for Sedimentary Geologists, Special Publicatrion 54, 3–21.

Compston, W., Williams, I.S., Myer, C., 1984. U–Pb geochronology of zircons from Lunar Breccia 73217 using a sensitive high mass-resolution ion-microprobe. Journal of Geophysical Research 89 (Supplement), B525–B534.

Compston, W., Williams, I.S., Kirschvink, J.L., Zhang, Z., Ma, G., 1992. Zircon U–Pb ages for the Early Cambrian time scale. Journal of the Geological Society of London 149, 171–184.

Condie, K.C., 1991. Precambrian granulites and anorogenic granites: are they related? Precambrian Research 51, 161–172.

Corfu, F., Hanchar, J.M., Hoskin, P.W.O., Kinny, P., 2003. Atlas of zircon textures. In: Hanchar, J., Hoskin, P.W.O. (Eds.), Zircon. Reviews in Mineralogy and Geochemistry, 53. Mineralogical Society of America, pp. 469–500.

De Laeter, J.R., Kennedy, A.K., 1998. A double focusing mass spectrometer for geochronology. International Journal of Mass Spectrometry 178, 43–50.

Degtyarev, K.E., 2003. Position of the Aktau–Dzhungar microcontinent in the structural framework of the Paleozoides of Central Kazakhstan. Geotectonics 37, 271–288.

Demoux, A., Kröner, A., Liu, D., Badarch, G., 2009. Precambrian crystalline basement in southern Mongolia as revealed by SHRIMP zircon dating. International Journal of Earth Sciences 98, 1365–1380.

DePaolo, D.J., 1988. Neodymium Isotope Geochemistry. Springer Verlag, Berlin, p. 187.

Djenchuraeva, R.D., Borisov, F.I., Pak, N.T., Malyukova, N.N., 2008. Metallogeny and geodynamics of the Aktiuz–Boordu Mining District, Northern Tien Shan, Kyrgyzstan. Journal of Asian Earth Sciences 32, 280–299.

Eby, G.N., 1992. Chemical subdivision of the A-type granitoids: petrogenetic and tectonic implications. Geology 20, 641–644.

Elvevold, S., Gilotti, J.A., 2000. Pressure–temperature evolution of retrogressed kyanite eclogites, Weinschenk Island, North-East Greenland Caledonides. Lithos 53, 127–147.

Filatova, L.I., 1993. Early Precambrian of Kazakhstan, North and Middle Tianshan. In: Kozakov, I.K. (Ed.), Early Precambrian of the Central Asia Folded Belt. Nauka, St. Petersburg, pp. 24–81 (in Russian).

Filippova, I.B., Bush, V.A., Didenko, A.N., 2001. Middle Paleozoic subduction belts: the leading factor in the formation of the Central Asian fold-and-thrust belt. Russian Journal of Earth Sciences 3, 405–426.

Frost, B.R., Barnes, C.G., Collins, W.J., Arculus, R.J., Ellis, D.J., Frost, C.D., 2001. A geochemical classification for granitic rocks. Journal of Petrology 42, 2033–2048.

Ghes', M.D., 2008. Terrane Structure and Geodynamic Evolution of the Caledonides of Tian Shan. Altyn Tamga Publishing House, Bishkek, p. 158 (in Russian).

Gladkochub, D.P., Donskaya, T.V., Wingate, M.T.D., Poller, U., Kröner, A., Fedorovsky, V.S., Mazukabzov, A.M., Todt, W., Pisarevsky, S.A., 2008. Petrology, geochronology, and tectonic implications of c. 500 Ma metamorphic and igneous rocks along the northern margin of the Central Asian Orogen (Olkhon terrane, Lake Baikal, Siberia). Journal of the Geological Society of London 165, 235–246.

Glorie, S., De Grave, J., Buslov, M.M., Elburg, M.A., Stockli, D.F., Gerdes, A., Van den haute, P., 2010. Multi-method chronometric constraints on the evolution of the Northern Kyrgyz Tien Shan granitoids (Central Asian Orogenic Belt): from emplacement to exhumation. Journal of Asian Earth Sciences 38, 131–146.

Glorie, S., De Grave, J., Buslov, M.M., Zhimulev, F.I., Izmer, A., Vandoorne, W., Ryabinin, A., Van Den hautre, P., Vanhaecke, F., Elburg, M.A., 2011. Formation and Paleozoic evolution of the Gorny–Altai–Mongolia suture zone (South Siberia): zircon U/Pb constraints on the igneous record. Gondwana Research. doi:10.1016/j.gr.2011.03.003.

Griffin, W.L., Pearson, N.J., Belousova, E., Jackson, S.E., van Achterbergh, E., O'Reilly, S.Y., Shee, S.R., 2000. The Hf isotope composition of cratonic mantle: LAM-MC-ICPMS analysis of zircon megacrysts in kimberlites. Geochimica et Cosmochimica Acta 64, 133–147.

Griffin, W.L., Belousova, E.A., Shee, S.R., Pearson, N.J., O'Reilly, S.Y., 2004. Archean crustal evolution in the northern Yilgarn Craton: U-Pb and Hf-isotope evidence from detrital zircons. Precambrian Research 131, 231–282.

Hegner, E., Klemd, R., Kröner, A., Corsini, M., Alexeiev, D.V., Iaccheri, L.M., Zack, T., Dulski, P., Xia, X., Windley, B.F., 2010. Chronology and P–T conditions of late Paleozoic high-pressure metamorphism and provenance of mélange sediments in the South Tianshan orogen of Kyrgyzstan. American Journal of Science 310, 916–950.

Hoffmann J.E., Münker C., Polat A., Rosing M.T., in press. The origin of decoupled Hf–Nd isotope compositions in early Archean rocks from southern West Greenland. Geochimica et Cosmochimica Acta.

Katayama, I., Maruyama, S., Parkinson, C.D., Terada, K., Sano, Y., 2001. Ion microprobe U-Pb zircon geochronology of peak and retrograde stages of ultrahigh-pressure metamorphic rocks from the Kokchetav massif, northern Kazakhstan. Earth Planetary Science Letters 188, 185–198.

Keller, B.M., Rukavishnikova, T.B., 1961. Tremadocian and adjacent deposits of the Kendyktas Range. In: Shatsky, N.S. (Ed.), Ordovician of Kazakhstan IV, Transactions of the Geological Institute, 18, pp. 22–28. Almaty (in Russian).

Kinny, P.D., 1986. 3820 Ma zircons from a tonalitic Amitsoq gneiss in the Godthab district of southern West Greenland. Earth and Planetary Science Letters 79, 337–347.

Kiselev, V.V., 1999. Uranium–lead (on zircon) geochronology of magmatic complexes of North Tianshan. Izvestiya NAN KR Special issue, pp. 21–33 (in Russian).

Kiselev, V.V., Maksumova, R.A., 2001. Geology of the Northern and Middle Tien Shan: principal outlines. In: Seltmann, R., Jenchuraeva, R. (Eds.), Paleozoic Geodynamics and Gold Deposits in the Kyrgyz Tien Shan. IAGOD Guidebook Series, 9. Natural History Museum, London, pp. 21–28.

Kiselev, V.V., Apayarov, F.Kh., Komartsev, V.T., Tsyganok, E.N., Lukashova, E.M., 1993. Isotopic ages of zircons from crystalline complexes of the Tianshan. In: Kozakov, I.K. (Ed.), Early Precambrian of the Central Asia Folded Belt. Nauka, St. Peterburg, pp. 99–115 (in Russian).

Konopelko, D., Biske, G., Seltmann, R., Kiseleva, M., Matukov, D., Sergeev, S., 2008. Deciphering Caledonian events: timing and geochemistry of the Caledonian magmatic arc in the Kyrgyz Tien Shan. Journal of Asian Earth Sciences 32, 131–141.

Koppers, A.A.P., 2002. ArArCALC-software for $^{40}Ar/^{39}Ar$ age calculations. Computers and Geosciences 28, 605–619.

Korobkin, V.V., Smirnov, A.V., 2006. Paleozoic tectonics and geodynamics of volcanic arcs in Northern Kazakhstan. Russian Geology and Geophysics 47 (4), 458–470.

Kozakov, K., Glebovitsky, V.A., Bibikova, E.V., Azimov, P. Ya., Kirnozova, T.I., 2002. Hercynian granulites of Mongolian and Gobian Altai: Geodynamic setting and formation conditions. Doklady Earth Sciences 386, 781–785.

Koslovskii, V.M., Aranovich, L.Ya., 2010. Petrology and thermobarometry of eclogite rocks in the Krasnaya Guba dike field, Belomorian mobile belt. Petrology 18, 27–49.

Kozlovsky, V.M., Aranovich, L.Ya., 2008. Geological and structural conditions of eclogitization of Paleoproterozoic basic dikes in the eastern Belomorian mobile belt. Geotectonics 42, 305–317.

Kröner, A., Wilde, S.A., Li, J.H., Wang, K.Y., 2005. Age and evolution of a late Archean to early Palaeoproterozoic upper to lower crustal section in the Wutaishan/Hengshan/Fuping terrain of northern China. Journal of Asian Earth Sciences 24, 577–596.

Kröner, A., Wilde, S.A., Zhao, G.C., O'Brien, P.J., Sun, M., Liu, D.Y., Wan, Y.S., Liu, S.W., Guo, J.H., 2006. Zircon geochronology of mafic dykes in the Hengshan Complex of northern China: evidence for late Palaeoproterozoic rifting and subsequent high-pressure event in the North China Craton. Precambrian Research 146, 45–67.

Kröner, A., Windley, B.F., Badarch, G., Tomurtogoo, O., Hegner, E., Jahn, B.M., Gruschka, S., Khain, E.V., Demoux, A., Wingate, M.T.D., 2007. Accretionary growth and crust-formation in the Central Asian orogenic belt and comparison with the Arabian–Nubian shield. In: Hatcher, R.D., Carlson, M.P., McBride, J.H., Martínez Catalán, J.R. (Eds.), 4-D Framework of Continental Crust: Geological Society of America Memoirs, 200, pp. 181–209.

Kröner, A., Alexeiev, D.V., Hegner, E., Corsini, M., Mikolaichuk, A., Xia, X., Zack, T., Windley, B.F., Sun, M., Rojas-Agramonte, Y., Liu, D., 2009. New zircon, Sm–Nd, and Ar–Ar ages for Precambrian and Palaeozoic rocks from the Tianshan orogenic belt in Kyrgyzstan and disappearance of the Archaean. International Field Excursion and Workshop on Tectonic Evolution and Crustal Structure of the Paleozoic Chinese Tianshan, Urumqi, China, September 9–19, 2009, pp. 43–44.

Kröner, A., Santosh, M., Wong, J., 2012. Zircon ages and Hf isotopic systematics reveal vestiges of Mesoproterozoic to Archaean crust within the late Neoproterozoic-Cambrian high-grade terrain of southernmost India. Gondwana Research 21, 876–886 (this issue).

Larsen, E.S., Keevil, N.B., Harrison, H.C., 1952. Method for determining the age of igneous rocks using the accessory minerals. Geological Society of America, Bulletin 63, 1045–1052.

Lee, J.-Y., Marti, K., Severinghaus, J.P., Kawamura, K., Yoo, H.-S., Lee, J.B., Kim, J.S., 2006. A redetermination of the isotopic abundances of atmospheric Ar. Geochimica et Cosmochimica Acta 70, 4507–4512.
Letnikov, F.A., Kotov, A.B., Salnikova, E.B., Shershakova, M.M., Shershakov, A.V., Rizvanova, N.G., Makeev, A.F., 2007. Granodiorites of the Grenville phase in the Kokchetav Block, Northern Kazakhstan. Doklady Earth Sciences 8, 1195–1197.
Li, X.H., 1997. Geochemistry of the Longsheng Ophiolite from the southern margin of Yangtze Craton, SE China. Geochemical Journal 31, 323–337.
Lomize, M.G., Demina, L.I., Zarshchikov, A.A., 1997. The Kyrgyz–Terskei Paleoceanic Basin. Tien Shan. Geotectonics 31, 463–482.
Long, X., Yuan, C., Sun, M., Kröner, A., Zhao, G., Wilde, S., 2011. Reworking of the Tarim Craton by underplating of mantle plume-derived magmas: evidence from Neoproterozoic granitoids in the Kuluketage area, NW China. Precambrian Research 187, 1–14.
Lu, S., Li, H., Zhang, C., Niu, G., 2008. Geological and geochronological evidence for the Precambrian evolution of the Tarim Craton and surrounding continental fragments. Precambrian Research 160, 94–107.
Mikolaichuk, A.V., Kurenkov, S.A., Degtyarev, K.E., Rubtsov, V.I., 1997. Northern Tien-Shan, main stages of geodynamic evolution in the late Precambrian and early Palaeozoic. Geotectonics 31, 445–462.
Miyashiro, A., 1974. Volcanic rock series in island arcs and continental margins. American Journal of Science 274, 321–355.
Mossakovsky, A.A., Ruzhentsev, S.V., Samygin, S.G., Kheraskova, T.N., 1993. Central Asian fold belt, geodynamic evolution and formation history. Geotectonics 27, 445–473.
Myers, J.S., 1978. Formation of banded gneisses by deformation of igneous rocks. Precambrian Research 6, 43–64.
Nakamura, N., 1974. Determination of REE, Ba, Fe, Mg, Na and K in carbonaceous and ordinary chondrites. Geochimica et Cosmochimica Acta 38, 757–775.
Nelson, D.R., 1997. Compilation of SHRIMP U–Pb zircon geochronology data, 1996. Geological Survey of Western Australia, Record 1997, 2, p. 189.
Nikitin, I.F., 1972. Ordovician of Kazakhstan. Part 1, Stratigraphy. Nauka, Alma-Ata, 242 p. (in Russian).
O'Brien, P.J., Walte, N., Li, J.H., 2005. The petrology of two distinct Paleoproterozoic granulite types in the Hengshan Mts., North China craton, and tectonic implications. Journal of Asian Earth Sciences 24, 615–627.
O'Connor, J.T., 1965. A classification for quartz-rich igneous rocks based on feldspar ratios. U.S. Geological Survey Professional Paper, B525, pp. 79–84.
Orozbaev, R.T., Takasu, A., Tagiri, M., Bakirov, A.B., Sakiev, K.S., 2007. Polymetamorphism of Aktyuz eclogites (northern Kyrgyz Tien-Shan) deduced from inclusions in garnets. Journal of Mineralogical and Petrological Sciences 102, 150–156.
Orozbaev, R.T., Takasu, A., Bakirov, A.B., Tagiri, M., Sakiev, K.S., 2010. Metamorphic history of eclogites and country rock gneisses in the Aktyuz area, Northern Tien-Shan, Kyrgyzstan: a record from initiation of subduction through to oceanic closure by continent–continent collision. Journal of Metamorphic Geology 28, 317–339.
Osmonbetov, K.O., 1980. Geological Map of the Kyrgyz SSR. VSEGEI, Leningrad. scale 1:500,000, in Russian.
Parkinson, C.D., Katayama, I., Liou, J.G., Maruyama, S. (Eds.), 2002. The diamond-bearing Kokchetav Massif, Kazakhstan. Universal Academic Press, Tokyo. 527 pp.
Passchier, C.W., Myers, J.S., Kröner, A., 1990. Field Geology of High-grade Gneiss Terrains. Springer-Verlag, Berlin, p. 150.
Pearce, J.A., Harris, N.W., Tindle, A.G., 1984. Trace element discrimination diagrams for the tectonic interpretation of granitic rocks. Journal of Petrology 25, 956–983.
Phillips, G., Landenberger, B., Belousova, E.A., 2011. Building the New England Batholith, eastern Australia—linking granite petrogenesis with geodynamic setting using Hf isotopes in zircon. Lithos 122, 1–12.
Qian, Q., Gao, J., Klemd, R., He, G., Song, B., Liu, D., Xu, R., 2009. Early Paleozoic tectonic evolution of the Chinese South Tianshan Orogen: constraints from SHRIMP zircon U–Pb geochronology and geochemistry of basaltic and dioritic rocks from Xiate, NW China. International Journal of Earth Sciences 98, 551–569.
Renne, P.R., Deino, A.L., Hames, W.E., Heizler, M.T., Hemming, S.R., Hodges, K.V., Koppers, A.A.P., Mark, D.F., Morgan, L.E., Phillips, D., Singer, B.S., Turrin, B.D., Villa, I.M., Villeneuve, M., Wijbrans, J.R., 2009. Data reporting norms for $^{40}Ar/^{39}Ar$ geochronology. Quaternary Geochronology 4, 346–352.
Rojas-Agramonte, Y., Kröner, A., Demoux, A., Xia, X., Wang, W., Donskaya, T., Liu, D., Sun, M., 2011. Detrital and xenocrystic zircon ages from Neoproterozoic to Paleozoic arc terranes of Mongolia: significance for the origin of crustal fragments in the Central Asian Orogenic Belt. Gondwana Research 19, 751–763.
Rudnik, R.L., 1995. Making continental crust. Nature 378, 571–578.
Ryazantsev, A.V., Degtyarev, K.E., Kotov, A.B., Sal'nikova, E.B., Anisimova, I.V., Yakovleva, S.Z., 2009. Ophiolite sections of the Dzhalair–Nayman zone, South Kazakhstan: their structure and age substantiation. Doklady Earth Science 427A, 902–906.
Salnikova, E.B., Kozakov, I.K., Kotov, A.B., Kröner, A., Todt, W., Bibikova, E.V., Nutman, A., Yakovleva, S.Z., Kovach, V.P., 2001. Age of Palaeozoic granites and metamorphism in the Tuvino-Mongolian Massif of tha Central Asian Mobile belt: loss of a Precambrian microcontinent. Precambrian Research 110, 143–164.
Scherer, E., Münker, C., Mezger, K., 2001. Calibration of the Lutetium–Hafnium clock. Science 293, 683–687.
Shatsky, V.S., Jagoutz, E., Sobolev, N.V., Kozmenko, O.A., Parkhomenko, V.S., Troesch, M., 1999. Geochemistry and age of ultrahigh pressure metamorphic rocks from the Kokchetav massif (Northern Kazakhstan). Contributions to Mineralogy and Petrology 137, 185–205.
Smelov, A.P., Beryozkin, V.I., 1993. Retrograded eclogites in the Olekma granite–greenstone region, Aldan Shield, Siberia. Precambrian Research 62, 419–430.
Steiger, R.H., Jäger, E., 1977. Subcommission on geochronology: convention of the use of decay constants in geo- and cosmochronology. Earth and Planetary Science Letters 36, 359–362.
Stevens, G., Villaros, A., Buick, I.S., Clemens, J.D., 2011. The Genetic Code for Granite. 23rd Colloquium of African Geology, abstract-volume. University of Johannesburg, p. 372.
Storey, C., 2008. The Glenelg-Attadale Inlier, NW Scotland, with emphasis on the Precambrian high-pressure metamorphic history and subsequent retrogression: an introduction and review. Scottish Journal of Geology 44, 1–16.
Tagiri, M., Yano, T., Bakirov, A., Nakajima, T., Uchiumi, S., 1995. Mineral parageneses and metamorphic P–T paths of ultrahigh-pressure eclogites from Kyrgyzstan Tien-Shan. The Island Arc 4, 280–292.
Tagiri, M., Takiguchi, S., Ishida, C., Noguchi, T., Kimura, M., Bakirov, A., Sakiev, K., Takahashi, M., Takasu, A., Bakirov, A., Togonbaeva, A., Suzuki, A., 2010. Intrusion of UHP metamorphic rocks into the upper crust of Kyrgyzian Tien-Shan: P–T path and metamorphic age of the Makbal Complex. Journal of Mineralogical and Petrological Sciences 105, 233–250.
Taylor, S.R., McLennan, S.M., 1985. The Continental Crust, Its Composition and Evolution. Blackwell, Oxford, p. 312.
Togonbaeva, A., Takasu, A., Bakirov, A.A., Sakurai, T., Tagiri, M., Bakirov, A.B., Sakiev, K., 2009. CHIME monazite ages of garnet-chloritoid-talc schist in the Makbal complex, Northern Kyrgyz Tien-Shan, first report of the age of the UHP metamorphism. Journal of Mineralogical and Petrological Sciences 104, 77–81.
Turner, G., Huneke, J.C., Podosek, F.A., Wasserburg, G.J., 1971. ^{40}Ar-^{39}Ar ages and cosmic ray exposure ages of Apollo 14 samples. Earth and Planetary Science Letters 12, 19–35.
Vervoort, J.D., Patchett, P.J., Soderlund, U., Baker, M., 2004. Isotopic composition of Yb and the determination of Lu concentrations and Lu/Hf ratios by isotope dilution MC-ICP-MS. Geochemistry Geophysics Geosystems 5, Q11002. doi:10.1029/2004GC000721.
Villaros, A., Buick, I.S., Stevens, G., 2011. Isotopic variations in S-type granites: an inheritance from the source — example from the Cape Granite suite. 23rd Colloquium of African Geology, abstract-volume. University of Johannesburg, South Africa, p. 416.
Whalen, J.B., Currie, K.L., Chappell, B.W., 1987. A-type granites: geochemical characteristics, discrimination and petrogenesis. Contributions to Mineralogy and Petrology 95, 407–419.
Whalen, J.B., Jenner, G.A., Currie, K.L., Barr, S.M., Longstaffe, F.J., Hegner, E., 1994. Geochemical and isotopic characteristics of granitoids of the Avalon Zone, southern New Brunswick: possible evidence for repeated delamination events. Journal of Geology 102, 269–282.
Williams, I.S., 1998. U–Th–Pb geochronology by ion microprobe. In: McKibben, M.A., Shanks III, W.C., Ridley, W.I. (Eds.), Applications of microanalytical techniques to Understanding mineralizing processes: Reviews in Economic Geology, 7, pp. 1–35.
Windley, B.F., Alexeiev, D.V., Xiao, W., Kröner, A., Badarch, G., 2007. Tectonic models for accretion of the Central Asian Orogenic Belt. Journal of the Geological Society, London 164, 31–47.
Xia X.P., Sun M., Sun Y.L., Wang Y.J., Zhao G.C., in press. Simultaneous determination of U–Pb and Hf isotope compositions of zircon by excimer laser-ablation multiple-collector ICPMS. Journal of Analytical Atomic Spectrometry 26.
Zonenshain, L.P., Kuzmin, M.I., Natapov, L.M., 1990. Geology of the USSR. A Plate Tectonic Synthesis. American Geophysical Union. Geodynamics Series, 21, p. 242.